JACS Au
AN OPEN ACCESS JOURNAL OF THE AMERICAN CHEMICAL SOCIETY

pubs.acs.org/jacsau
Perspective

Chemical Upcycling of Polyolefin Plastics Using Structurally Well-defined Catalysts

Simin Sun and Wenyu Huang*

Cite This: JACS Au 2024, 4, 2081−2098
Read Online
ACCESS | Metrics & More | Article Recommendations

ABSTRACT: Single-use polyolefins are widely used in our daily life and industrial production due to their light weight, low cost, superior stability, and durability. However, the rapid accumulation of plastic waste and low-profit recycling methods resulted in a global plastic crisis. Catalytic hydrogenolysis is regarded as a promising technique, which can effectively and selectively convert polyolefin plastic waste to value-added products. In this perspective, we focus on the design and synthesis of structurally well-defined hydrogenolysis catalysts across mesoscopic, nanoscopic, and atomic scales, accompanied by our insights into future directions in catalyst design for further enhancing catalytic performance. These design principles can also be applied to the depolymerization of other polymers and ultimately realize the chemical upcycling of waste plastics.

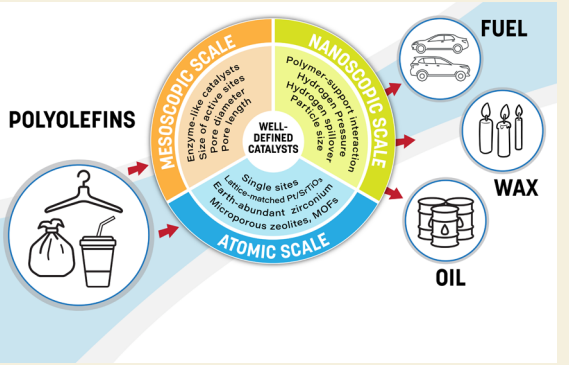

KEYWORDS: *recycling, polyolefin, catalytic hydrogenolysis, depolymerization*

INTRODUCTION

Due to the superior characteristics of plastics, including low cost, light weight, extreme stability, and good durability, the applications of plastics exceptionally improve the quality of our daily life in almost every aspect, such as better food preservation, one-time-use medical devices, corrosion-resistant pipes, cheap and lightweight packaging materials, etc. Unfortunately, the increasing demands, low cost, and mostly one-time-use nature of plastics result in a rapid accumulation of plastic waste.[1] Among 353 million tons (Mt) of plastic waste generated in 2019, only 9% of plastics were recycled, while 19% were incinerated, 22% were leaked into the environment due to mismanagement, and the remainder ended up in landfills,[2] which poses a potential threat to our environment and, ultimately, to human health. There are several recycling methods to overcome the plastic waste crisis: mechanical recycling (primary and secondary), chemical recycling (tertiary), and incineration (quaternary).[3] Mechanical recycling involves two main steps: grinding and remodeling the plastics into new products. The difference between primary and secondary recycling is that the former uses postindustrial plastic wastes as the substrate, while the latter uses postconsumer plastics. However, both methods produce downgraded polymer products that are finally dumped into landfills.[4] Incineration can only partially recover the energy used to produce plastics and also generates a tremendous amount of greenhouse gases and pollutants, like the microplastic residues in the ashes.[5] Chemical recycling is considered the most promising method that can convert plastic waste into value-added products, also termed chemical upcycling.[6−12] However, chemical recycling and upcycling could be more energy-intensive and expensive to implement in industry than mechanical recycling and incineration.[4] Hence, developing more efficient and incentivized chemical conversion processes could significantly reshape the lifecycle of plastics.

Globally, the production of polyolefin (PO), including polyethylene (PE) and polypropylene (PP), reached 105 and 76 Mt in 2022, respectively, accounting for approximately 50% of the total plastic commodity market.[13] To solve the plastic waste crisis, this large body of PO plastics must be recycled in an efficient circular pathway or repurposed into high-value products, which inevitably involves depolymerization of PO. Depolymerizing PO to high-value chemicals requires selectively breaking C−C bonds. However, the saturated C−C bonds in the PO backbone are stable and cannot be cleaved easily.[14] Pyrolysis and hydrocracking are conventional chemical recycling and upcycling methods for PO that can obtain gaseous and liquid products. However, the pyrolysis reaction is typically endothermic and requires high temperatures (>400 °C),[15,16] which increases energy cost of the process and

Received: March 31, 2024
Revised: May 12, 2024
Accepted: May 17, 2024
Published: June 4, 2024

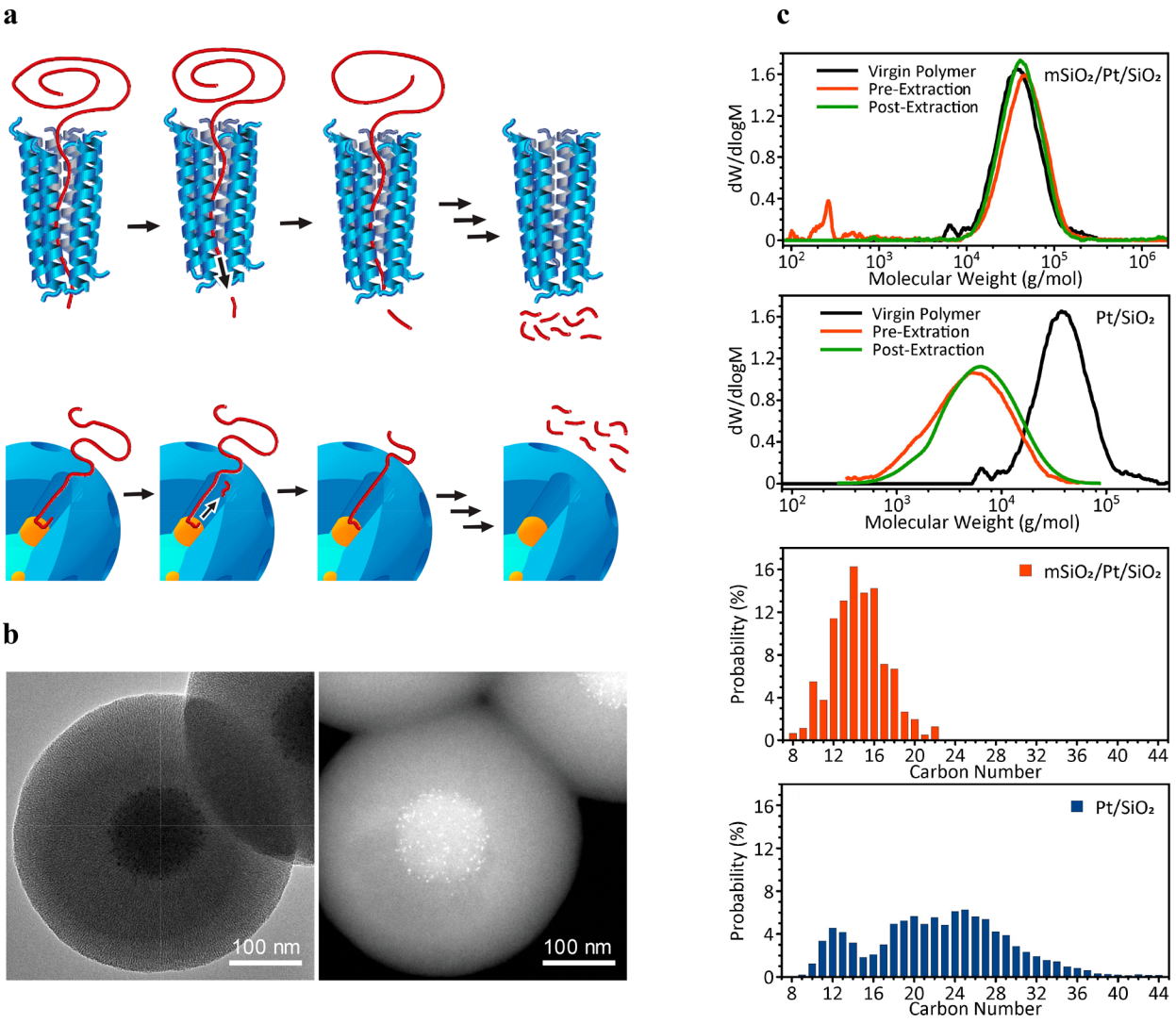

Figure 1. Porous core−shell structure and processivity of enzyme-like $mSiO_2/Pt/SiO_2$. (a) A processive mechanism proposed for $mSiO_2/Pt/SiO_2$, analogous to the mechanism that many enzymes deconstruct large macromolecules. (b) Bright- and dark-field transmission electron microscopy of the $mSiO_2/Pt/SiO_2$. (a) and (b) were reproduced with permission from ref 30. Copyright 2020 Springer Nature. (c) Top: gel permeation chromatography (GPC) analysis of the molecular weight distribution of solid components before and after reaction by 220 nm $mSiO_2/Pt/SiO_2$ and Pt/SiO_2. Bottom: GC analysis of the distribution of liquid products by 220 nm $mSiO_2/Pt/SiO_2$ and Pt/SiO_2 (catalysis conditions: 50 mg of linear PE, M_n = 34.2 kDa; M_w = 42.4; $Đ$ = 1.24, 300 psi H_2, 300 °C, 12 h). Reproduced with permission from ref 31. Copyright 2023 American Chemical Society.

simultaneously lowers product selectivity.[17,18] More thermodynamically favorable hydrocracking can be carried out at lower temperatures (250−375 °C) than pyrolysis,[5] but it leads to heavily isomerized branching alkane products.[19,20] Compared to pyrolysis and hydrocracking, catalytic hydrogenolysis is usually exothermic,[21] which can convert PO into more desirable linear alkane products under milder conditions (≤300 °C).[22] The H_2-rich environment during hydrogenolysis can promote the cleavage of C−C bonds, the hydrogenation of intermediates to form alkanes, and the suppression of coke deposition and isomerization, the main obstacle of pyrolysis and hydrocracking.[17−20,22,23]

Previous studies on C−C hydrogenolysis were mostly carried out on small alkanes in the gas phase. This could be very different from PO hydrogenolysis, which needs to be carried out in the condensed phase. Therefore, fundamental understanding and catalytic process development of the C−C hydrogenolysis in PO are urgently needed. Due to the similarities in the C−C bonds in the PO backbone, controlling selectivity in C−C cleavage represents the most challenging topic in PO hydrogenolysis. Catalyst design could play a significant role in controlling product alkane chain length and preventing the formation of gases, especially methane, which are important to increase the value of the products and make the recycling and upcycling of waste PO plastics profitable for broad adoption.

Compared to small molecule catalysis, where the reactant typically has a well-defined composition, polymer deconstruction reactions involve a mixture of molecules with a broad molecular weight distribution. Consequently, it is challenging to accurately monitor changes in reactants, reaction intermediates, and catalysts due to the complexity of the reaction. The interaction between the molecule and the active site is crucial in small-molecule catalysis. However, in the case of large polymer molecules, the interaction between the molecule and the heterogeneous catalyst support could also

https://doi.org/10.1021/jacsau.4c00289
JACS Au 2024, 4, 2081−2098

play a significant role in determining activity and selectivity. Therefore, designing structurally well-defined catalysts is critical for the chemical upcycling of waste plastics as it helps to modulate both the polymer−active site and polymer−support interaction. There have been reviews on PO hydrogenolysis that summarize the recent developments in catalysts and catalytic processes.[16,22,24−27] Some reviews also list catalysts with their compositions, catalysis conditions, and major products.[10,24,26,27] Herein, we focus on interpreting the crucial roles of structurally well-defined catalysts at mesoscopic, nanoscopic, and atomic scales in advancing our fundamental understanding and improving the catalytic activity and selectivity of PO hydrogenolysis. We also give our perspective on designing and synthesizing structurally well-defined catalysts that could further improve their catalytic performance in PO hydrogenolysis. Similar catalyst design principles should also be applicable to the deconstruction of other natural or manmade polymers.

CATALYSTS WITH WELL-DEFINED MESOSCOPIC STRUCTURES

The connection between natural enzymes and the design of well-defined catalysts lies in the emulation of the precise active site architecture exhibited in enzymes, which ingeniously combine specific binding sites (localized areas that control bond breaking or making) with precisely positioned nonreactive components, which promote access to binding sites and influence reaction dynamics.[28] The design of robust enzyme-like catalysts, precisely placing both reacting and nonreacting components, is beneficial to active and selective chemical transformations under challenging conditions.[28]

Well-defined Porous Core−Shell Catalysts for Processive Hydrogenolysis of PO

Processivity, initially proposed to describe the ability of natural enzymes to catalyze consecutive reactions without releasing their substrate, has been used in designing enzyme-like artificial catalysts.[29] The first implementation of the concept in designing inorganic heterogeneous catalysts was demonstrated by an ordered mesoporous silica shell/active sites/core architecture ($mSiO_2/Pt/SiO_2$), Figure 1a.[30] This innovative three-layer catalyst was synthesized by localizing 3.2 ± 0.5 nm Pt nanoparticles (NPs) on amine-functionalized silica spheres (SiO_2, 127 ± 7 nm in diameter), followed by the growth of mesoporous silica shell ($mSiO_2$, 110 ± 8 nm in thickness) with radially organized pores (2.4 ± 0.2 nm in diameter) grown around silica spheres (Figure 1b). In $mSiO_2/Pt/SiO_2$, the thickness of the $mSiO_2$ shell was equivalent to the pore length and Pt NPs were precisely positioned at the end of linear channels in the $mSiO_2$ shell. These linear pores in the $mSiO_2$ shell controlled the linear conformation of PE chains when they entered the pores, validated by ^{13}C solid-state nuclear magnetic resonance (SSNMR). To thoroughly understand the significance of the porous structure, a control sample, Pt/SiO_2, was synthesized by supporting Pt NPs on silica spheres without growing the enclosing $mSiO_2$ shell, on which polymer chains would be adsorbed and cleaved randomly.

As expected, the hydrogenolysis of high-density polyethylene (HDPE) catalyzed by Pt/SiO_2 leads to significant changes in number-average molecular mass (M_n), weight-average molecular mass (M_w), and polydispersity ($Đ = M_w/M_n$) of the remaining HDPE fraction. However, the hydrogenolysis catalyzed by $mSiO_2/Pt/SiO_2$ gives the same molecular mass of the remaining HDPE as the starting HDPE (Figure 1c).[31] Furthermore, the short alkane products obtained on $mSiO_2/Pt/SiO_2$ exhibit a much narrower distribution than those obtained from Pt/SiO_2. These contrasting results indicate that during the hydrogenolysis catalyzed by $mSiO_2/Pt/SiO_2$, all reacting HDPE chains were thoroughly deconstructed to smaller, dichloromethane-soluble hydrocarbons. In contrast, the nonreacting HDPE chains were unaffected and maintained the same molecular mass as the starting HDPE. This behavior proved the processivity, where the small products effectively exited the mesopores, while long polymer chains were not released due to their relatively stronger interaction with the silica pores than small product molecules. A microkinetic model coupled with population balance models was proposed to predict the transformation of molecular weight distribution during deconstruction and simultaneously validate the processivity in the catalytic reactions, consistent with the results of UV−vis-based experiments that the adsorption behavior of hydrocarbon chains is molecular-weight dependent.[32,33] Compared with long polymer chains, shorter segments would not have a longer residence time in the pore, which prevents them from converting to gases through further C−C bond cleavages and enables the processivity of this mesoporous catalyst.[32] These results reveal that $mSiO_2/Pt/SiO_2$ can effectively mimic the catalytic behavior of natural enzymes and realize the processive cleavage of the C−C bonds in PO, as depicted in Figure 1a. This processive PE hydrogenolysis yields narrowly distributed alkane products. Processivity in the hydrocracking of HDPE has also been demonstrated by Ru/HZSM-5 catalysts.[34]

The Size Effects of Active Sites

Based on the mesoporous silica shell/active sites/core catalyst architecture of $mSiO_2/Pt/SiO_2$, the effects of Pt NP size on the activity and selectivity in PE hydrogenolysis were investigated.[35] Benefiting from the well-defined and controllable architecture of this catalyst platform, other structure parameters of the catalysts were kept identical, including the SiO_2 core diameter, the $mSiO_2$ shell thickness, and the pore diameter in the $mSiO_2$ shell. Three $mSiO_2/Pt\text{-}X/SiO_2$ catalysts (where X represents the mean NP diameter, X = 1.7, 2.9, 5.0 nm) show equivalent chain-length product distributions in hydrogenolysis of PE (M_n = 20 kDa, M_w = 90 kDa, ρ = 0.92 g/mL). However, the size of Pt NPs significantly influenced the rate of carbon−carbon cleavages, and smaller Pt NPs showed higher cleavage rates. Obviously, when the size of Pt NPs decreases, the ratio of edge/corner sites to facet sites increases, revealing PE hydrogenolysis rates are higher at edge/corner sites than facet sites of Pt NPs, further supporting that the hydrogenolysis reaction is structure sensitive. Notably, the $mSiO_2/Pt\text{-}X/SiO_2$ architecture templated the product distribution in PE hydrogenolysis rather than the size of Pt NPs. The adsorption of PE chains into mesopores controls the translocation and conformation of polymer chains, thereby influencing the product distributions. Additionally, although the pore diameter of 2.4 nm is larger than 1.7 nm Pt NPs, no postreaction aggregation or leaching of Pt NPs were observed, which means that the presence of $mSiO_2$ can effectively prevent the migration and detachment of Pt NPs from the SiO_2 support. This finding exhibits the importance and robustness of this ordered mesoscale architecture in PO hydrogenolysis.

https://doi.org/10.1021/jacsau.4c00289
JACS Au 2024, 4, 2081−2098

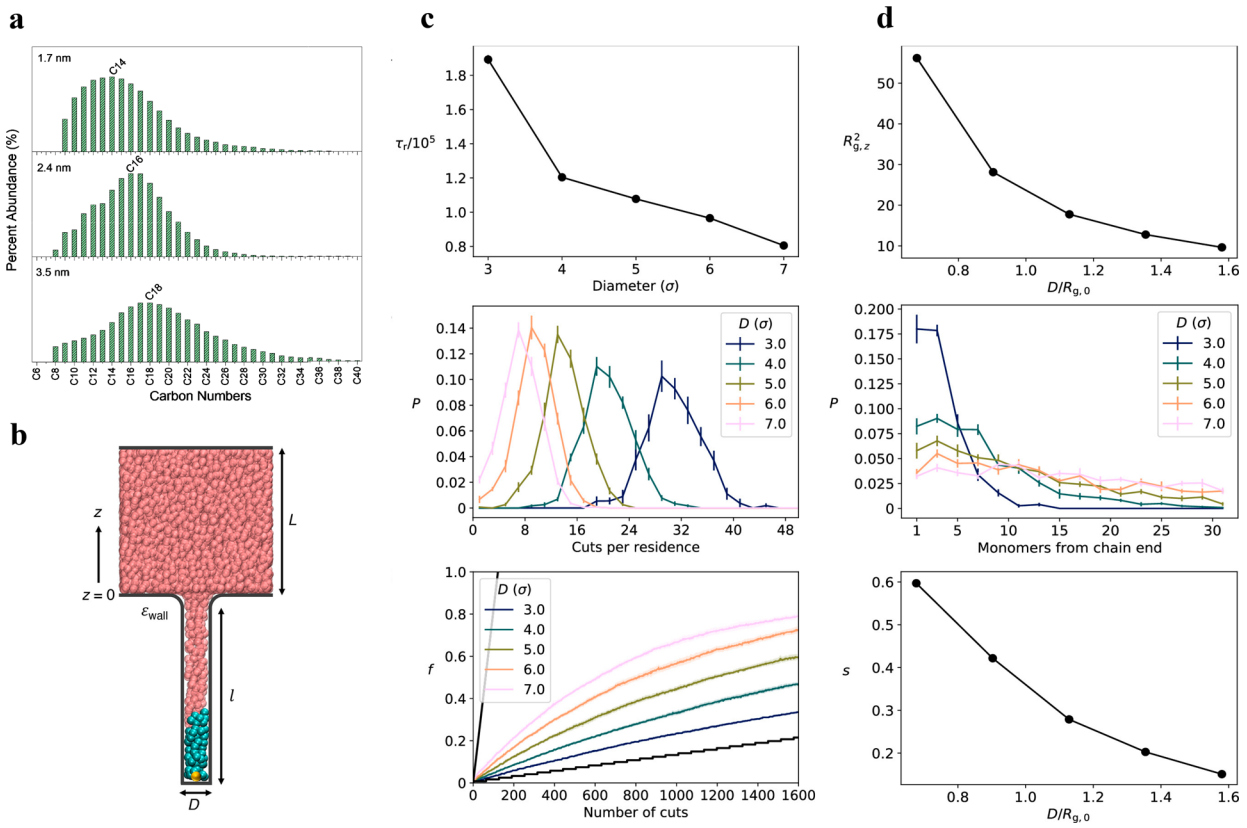

Figure 2. Pore diameter effects on PO hydrogenolysis. (a) Liquid product distributions obtained from HDPE hydrogenolysis at full conversion at 300 °C under 1.38 MPa H_2 for 24 h using $mSiO_2/Pt/SiO_2$ (0.004 wt % Pt with respect to HDPE) with pore diameters of 1.7 (top), 2.4 (middle), and 3.5 (bottom) nm. Reproduced with permission from ref 30. Copyright 2020 Springer Nature. (b) Schematic of the model system. A single chain of length $N = 64$ is highlighted in cyan. A representative pore with diameter $D = 4.0\sigma$ and length $l = 32\sigma$ is shown (with σ representing the monomer size). Catalysis reactions: PE (M_n = 20 kDa, M_w = 90 kDa, ρ = 0.92 g/mL), 0.89 MPa H_2, 300 °C for 6−20 h. (c) Effects of residence time on the cleavage of chains ($N = 64$) in a pore and its pore diameter dependence. Top: mean residence time τ_r of a chain as a function of pore diameter; center: probability distribution P of the number of times before the chain is cleaved before its fragments leave the pore; bottom: fraction f of the original chains that have been chopped at least once. (d) Effects of pore-diameter-dependent chain conformation on cleavage products and processivity. Top: average z-component $R^2_{g,z}$ of a chain ($N = 64$) before the cleavage as a function of pore diameter D; center: probability distribution P of the first bond cleaved in original chains; bottom: processivity of cleavage events s as a function of the pore diameter. (b) to (d) were reproduced with permission from ref 36. Copyright 2023 American Chemical Society.

The Effects of Pore Diameter

Keeping the same Pt NP diameter (~3.2 nm), SiO_2 core diameter (~127 nm), and $mSiO_2$ pore length (~110 nm), $mSiO_2/Pt/SiO_2$ with a small pore diameter of 1.7 nm results in a distribution predominantly of shorter C_{14}-centered hydrocarbons in PE hydrogenolysis, while a large pore diameter of 3.5 nm leads to longer C_{18}-centered products (Figure 2a).[30] To fully understand how the pore diameter influences product distributions, coarse-grained simulations were utilized to clarify the interaction between pore residence times and chain cleavages.[36] A model system was developed where a bulk polymer solution engages a planar substrate with a cylindrical, end-closed pore (Figure 2b). The investigation of the changes in M_w of products relative to pore diameter revealed that larger pores yield larger average products, consistent with experimental results. These observed diameter-dependent differences in product distributions were explained by two possible mechanisms. One is the dynamic mechanism, showing that the polymer residence time controls how many times the chain is cleaved if the C−C cleavage rate remains constant and is independent of the polymer length. Figure 2c exhibits the inverse relationship between the pore diameter and average residence time, which means the chains in broader pores have short residence times and are less frequently cleaved than in narrower pores. Interestingly, when the numbers of cuts are the same, broader pores give a larger fraction of cleaved initial chains than do narrower pores. Another mechanism is the structure mechanism. An enhanced C−C bond cleavage probability was observed for near-terminal C−C bonds, and the bias is predominantly dependent on pore diameter. In the narrower pores, the geometry adopts the elongated configuration of polymer chains. Figure 2d further illustrates how the pore diameter affects the processivity of catalytic reactions, in which s denotes the fraction of all successive cuts. The inverse relationship between s and pore diameters reveals that with increasing pore size, the probability of finding multiple chains near the catalyst increases, and the exchange of chains between the bulk and pore is more rapid. In summary, the analysis of chain residence times and preferred bond cleavages suggests that the product lengths depend on pore-diameter-dependent dynamics and conformational limitations.

The Effects of Pore Length

In addition to the pore diameter, the pore length also plays a vital role in the hydrogenolysis reactions. In situ, magic-angle spinning (MAS) NMR spectroscopy was used to elucidate the mechanism of processive PO hydrogenolysis.[31] To clarify the

https://doi.org/10.1021/jacsau.4c00289
JACS Au 2024, 4, 2081−2098

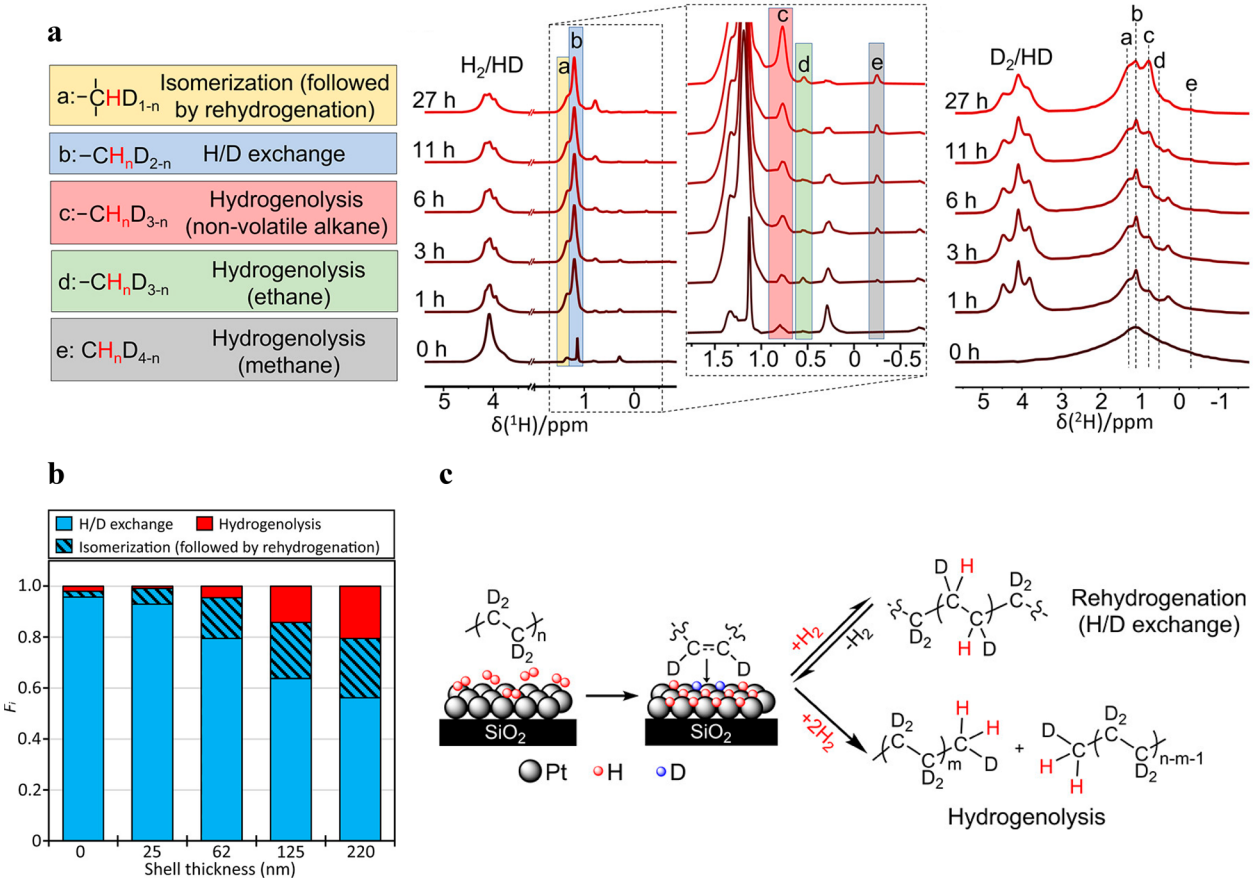

Figure 3. Pore length effects on the extent of processivity in PO hydrogenolysis. (a) In situ ^{1}H (left) and ^{2}H (right) NMR spectra obtained during a 27 h d_4-PE hydrogenolysis reaction catalyzed by a 125 nm $mSiO_2/Pt/SiO_2$ catalyst under 300 psi H_2 at 300 °C. The inset shows an enlarged view of the alkane region from the ^{1}H spectra. Resonances were assigned as indicated in the figure. (b) Normalized product fraction (F_i) after 27 h of reaction as a function of catalyst shell thickness. (c) Schematic depiction of the Pt/SiO_2-catalyzed d_4-PE hydrogenolysis mechanism and the formation of unique ^{1}H-containing products. Reproduced with permission from ref 31. Copyright 2023 American Chemical Society.

explanation of the mechanism, the definition of the extent of processivity needs to be elucidated, which is the average number of reactions of a reactant chain during its residence in the pore—the larger the extent of processivity, the less release of partially cleaved polymer intermediates back into the melt, and narrower product distributions. To explore the effect of the pore length on the processivity of the catalyst, X-$mSiO_2/Pt/SiO_2$ (X represents the pore length, equivalent to the thickness of the $mSiO_2$ shell) with different shell thicknesses were prepared. As shown in Figure 3c, the dehydrogenative chemisorption of a polymer chain creates M−H and M−C bonds on the metal NP surface. Then, hydrogen from NPs may be transferred to organometallic moieties in a reductive elimination, leading to the release of two shorter alkanes. As depicted in Figure 3a, the intensity of peaks b−e, corresponding to H/D exchange and hydrogenolysis, increased with time, confirming the occurrence of these two processes.

Interestingly, the H/D exchange signal was more intensive than the sum of various hydrogenolysis signals and grew much faster as the time increased from 0 to 27 h, which reveals that most PE−Pt interactions kinetically favored dehydrogenation/rehydrogenation and the release of polymer instead of cleavage of C−C bonds. Furthermore, to better evaluate how the shell thickness influences the probability of different reactions, the normalized product fraction after 27 h was calculated. Figure 3b shows that H/D exchange was still the predominant reaction for all pore lengths, but the fraction of hydrogenolysis significantly increased with the increase in pore length, proving that processivity corresponds to pore length. The molecular dynamics simulations further confirm that longer pores preferentially made the polymer chains entirely confined, increased the residence time in the pore, and increased the efficiency of cutting numbers per residence, which resulted in increasing processivity. Moreover, the degree of isomerization was also boosted in long pores due to increased polymer residence time.

The pore length not only affects the extent of processivity but also controls the chain length of products. A microkinetic model was created, assuming the polymer chain was partially confined within the pore.[37] The amount of consumed H_2 was equal to the number of C−C bond cleavages since each C−C bond cleavage consumes one equivalent of H_2, which is then divided by time to calculate the C−C bond cleavage rate. Interestingly, no matter whether the pore length was longer or shorter, the rates of C−C cleavage maintained equivalent, confirming that polymer mass transport inside the pores is not rate-limiting since the pores are filled all the time in the melted polymer. Likewise, the equivalent H_2 consumption with varying pore lengths suggests that the pore architecture did not limit H_2 diffusion. However, the product distributions of X-$mSiO_2/Pt/SiO_2$ at similar conversions differed. The 25-$mSiO_2/Pt/SiO_2$ yields a broader product distribution centered

https://doi.org/10.1021/jacsau.4c00289
JACS Au 2024, 4, 2081−2098

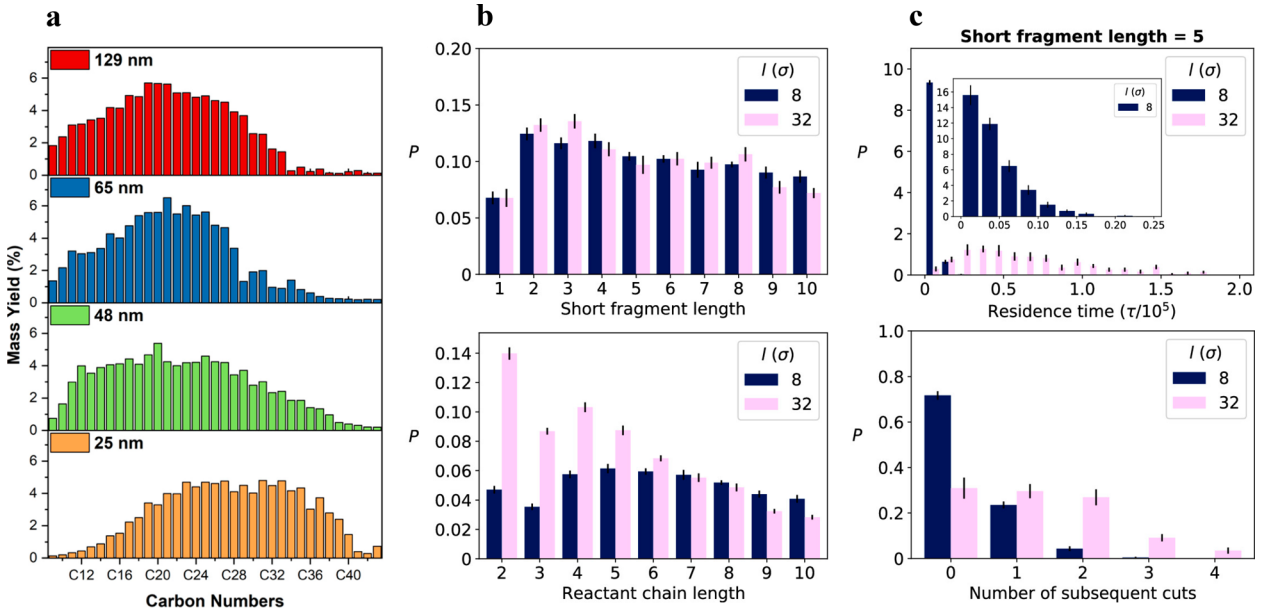

Figure 4. Pore length effects on product selectivity in PO hydrogenolysis. (a) Wax product distributions of X-mSiO$_2$/Pt/SiO$_2$ with the same numbers of C−C cleavages as measured by H_2 consumption. Reaction conditions: 3 g of PE-short (M_n = 2.8 kDa, M_w = 5 kDa) with 0.003 wt % Pt with respect to PE and 0.89 MPa H_2 at 300 °C for 6 h. (b) Difference between the length distributions of fragments (i.e., exclusively produced by cleaving longer chains) and all reactant chains from simulated data. Top: the probabilities of creating fragments of a given size chain; bottom: the probabilities of cleaving short chains. (c) Lifetime analysis of a representative (N = 5) short fragment within the pore from the simulation data. Top: distribution of intrapore residence times, and the inset shows the zoomed-in distribution for the shorter pore length ($l = 8\sigma$); bottom: distribution showing the number of cleaving times during a single residence. Reproduced with permission from ref 37. Copyright 2023 American Chemical Society.

at heavier hydrocarbons than other longer pore lengths (Figure 4a). To understand why longer pores lead to the formation of lighter hydrocarbons, one hypothesis is that the conformation of a polymer chain lies in whether it is partially or fully confined. The conformation of polymer chains can affect the bias of specific C−C bond cleavages. To examine this conformation effect, a chain with length $N > 10$ was utilized to monitor the length of short fragments after cleavages. Interestingly, no apparent differences in the frequencies of short fragment lengths were observed in the shortest ($l = 8\sigma$) and longest pores ($l = 32\sigma$), proving that the variations in pore length did not exert a substantial conformational impact on C−C bond cleavages (Figure 4b). Meanwhile, the distribution of reactant chain lengths shows that longer pores prefer to retain shorter reactants. It raises another hypothesis that the residence time controls average product length. Taking the reactant with length N = 5 as a representative, longer pores possess longer residence times of these reactants and thus increase the number of subsequent cuts, generating shorter products (Figure 4c). Hence, the pore length not only influences the extent of processivity but also affects the average length of products. Combined with the size effect of Pt NPs and pore diameter effects, these three essential parameters can be employed to optimize catalytic architecture and improve activity, selectivity, and stability in PO hydrogenolysis.

The Transformation from Open−Closed to Open−Open Architectures

The distinct design of mSiO$_2$/Pt/SiO$_2$ precisely located catalytic sites at the closed ends of mesopores. This porous architecture showed key characteristics of processivity, enabled the preferential release of products, restricted the overcutting of C−C bonds to form light gases, and effectively prevented catalytic sites from deactivation over nonporous architecture. The presence of "dead-end" pores, however, made a different dynamic from more common "open-pore" nature enzymes with catalytic sites at a defined distance from the pore end (Figure 5c).[38] Assuming a more open catalyst system can facilitate the leaving of products from active Pt sites and prevent the further cleavage of products to light gases including methane, mSiO$_2$/Pt/MCM-48 was prepared by positioning Pt NPs on the surface of the mesoporous MCM-48 core and then growing another layer of mSiO$_2$ shell. Remarkably, this catalyst depicted a C_{28}-centered Gaussian product distribution in deconstructing PO with faster C−C bond cleavage rates and negligible methane production (Figure 5a−b). The turnover frequency (TOF) is 4.2 ± 0.3 s^{-1}, much higher than solid-core catalyst mSiO$_2$/Pt/SiO$_2$ (1.6 ± 0.1 s^{-1}) and nonporous catalyst Pt/SiO$_2$ (1.3 ± 0.1 s^{-1}). Additionally, the involvement of a porous core provided pathways for fragments to diffuse away from cleavage sites and thereby avoided secondary reactions that led to the formation of volatiles, especially methane. With the same polymer to Pt ratio, Pt particle size, and reaction conditions, mSiO$_2$/Pt/MCM-48 converted 1.360 g of low-density polyethylene (LDPE, M_n = 20 kDa, M_w = 91 kDa) and produced 0.054 g (4%) of volatiles, including 0.0025 g of (0.18%) methane, while mSiO$_2$/Pt/SiO$_2$ only converted 0.424 g of LDPE, but produced 0.070 g (17%) of volatiles, including 0.0034 g (0.74%) of methane. The coarse-grained simulation indicates that the existence of end-opened pore facilitates the release of fragments and decreases the likelihood of overhydrogenolysis to generate shorter products (Figure 5d). Another interesting finding is that as time increased, a Gaussian C_{28}-centered distribution was shifted to a Gaussian C_{14}-centered distribution, meaning the bias on specific midchain C−C bond cleavages in short paraffin, which needs more explorations to clarify the mechanism behind this

https://doi.org/10.1021/jacsau.4c00289
JACS Au 2024, 4, 2081−2098

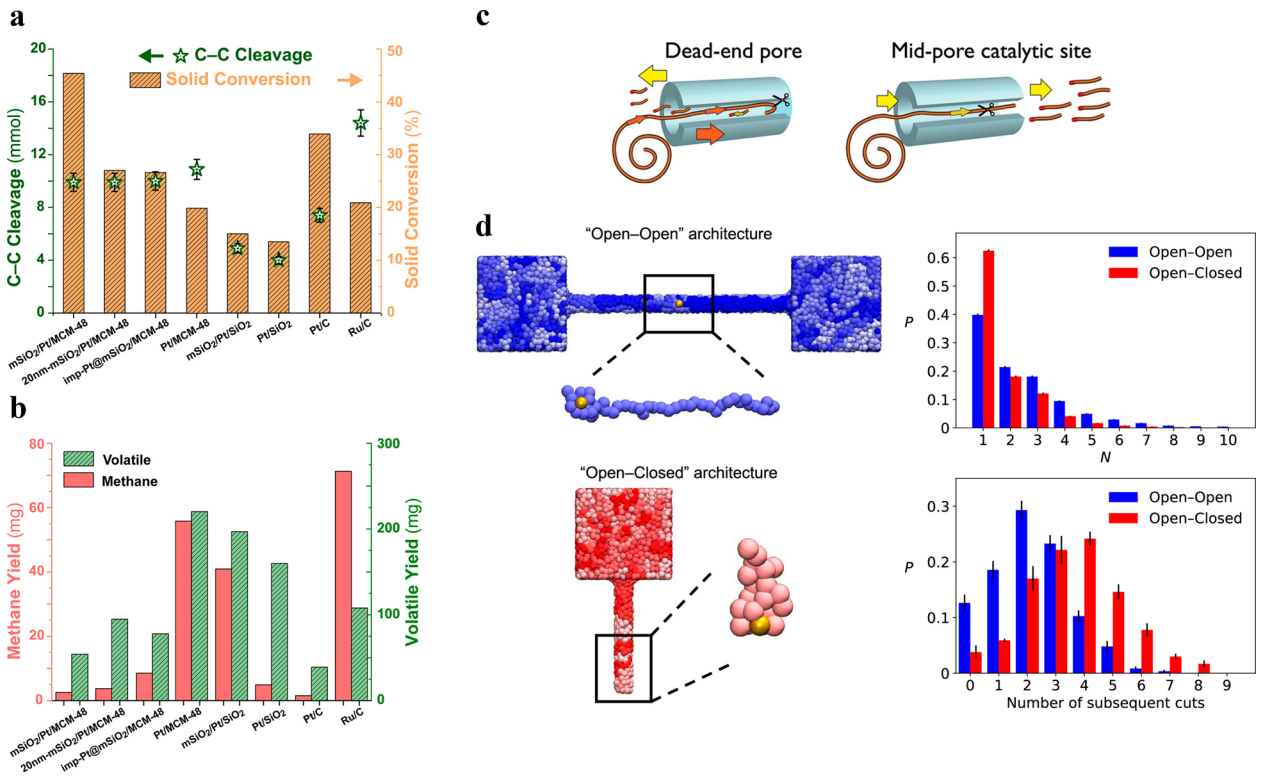

Figure 5. Comparisons between an "open−open" architecture and an "open−closed" architecture. (a) Catalytic performance of catalysts for LDPE (M_n = 20 kDa) conversion and C−C bond hydrogenolysis, under 2.06 MPa H_2 at 300 °C for 6 h using 0.0044 M/LDPE wt % (M = Pt, Ru). (b) Methane and total gas (C_1−C_7) formation after cleavage of ca. 10 mmol of C−C bonds in LDPE. (c) Sites for C−C bond cleavage (illustrated as pairs of scissors) at the end of an "open−closed" pore or in the middle of an "open−open" pore as the catalyst processively deconstructs a chain. (d) Molecular dynamics simulation results comparing the model cleavage products from an open−open architecture analogous to $mSiO_2$/Pt/MCM-48 to those from an open−closed architecture like $mSiO_2$/Pt/SiO_2. The cleavage site is represented by a gold-colored particle located at the center of the pore connecting the two bulk regions or fixed at the pore bottom. Reproduced with permission from ref 38. Copyright 2023 American Chemical Society.

phenomenon. The significant differences between an "open−closed" architecture and an "open−open" architecture reveal that a template effect can determine the product distribution in the polymer deconstruction, which means the scale dimensions and structural configuration of the mesoporous core and shell can be applied to optimize the selectivity of PO hydrogenolysis.

Perspectives

With the inspiration of natural processive enzymes, a series of inorganic processive catalysts are designed that effectively improve the catalytic activity and selectivity in PO hydrogenolysis. These enzyme-like catalysts realize the combination between binding sites (localized regions that promote bond breaking/making in the reacting molecule) and precise positioning of nonreacting components that influence reaction barriers and control access to the binding sites. To further optimize the performance of catalysts, one future direction is using crystalline microporous structures instead of amorphous mesoporous structures to mimic the atomic-level confined environment inside processive enzymes. Both experimental and coarse-grained, particle-based simulations have proved that pore diameter not only influences the residence time of a polymer chain near the active site, which controls how many times it is cleaved and final product distributions (narrower pore prefers to yield smaller products), but also affects the conformation of a polymer chain when it threads into the pore and accesses the active site. Crystalline microporous materials, such as zeolite and metal−organic frameworks (MOFs), could provide atomic-level defined pores to control the translocation and conformation of confined polymer chains. The MFI type zeolite could be an ideal choice of microporous core and shell (the pore size is around 0.50~0.55 nm) because the synthesis methodology has been mature, making it accessible to control the size and morphology of zeolite crystals. Catalytic active sites can be introduced into zeolite for cleaving C−C bonds, including metal NPs, small clusters, and single sites. Acid sites can also be introduced and adjusted by tuning the Si/Al ratio in zeolite, providing additional active sites for hydrocracking and isomerization of hydrocarbons. Although micropores can limit the conformation of polymer chains and bias which bonds are most likely to be cleaved, enhancing the selectivity of hydrogenolysis reactions, possible slow diffusion of polymer and products during the catalysis could be a main challenge, affecting the activity and selectivity of zeolite-supported catalysts in hydrogenolysis. Therefore, precisely controlling the depth of active sites from the surface of zeolite crystal is another future research direction. Similar approaches could also be extended to well-defined MOF structures, but the main challenge for applying MOFs in hydrogenolysis lies in the stability under harsh reaction conditions.

In addition to the inspiration from the processivity of natural enzymes, cooperativity, another common motif exhibited in enzymes, can also be used to guide the design and construction of multisite cooperative catalyst systems, which provide many possible combinations of types of active sites in synthetic

https://doi.org/10.1021/jacsau.4c00289
JACS Au 2024, 4, 2081−2098

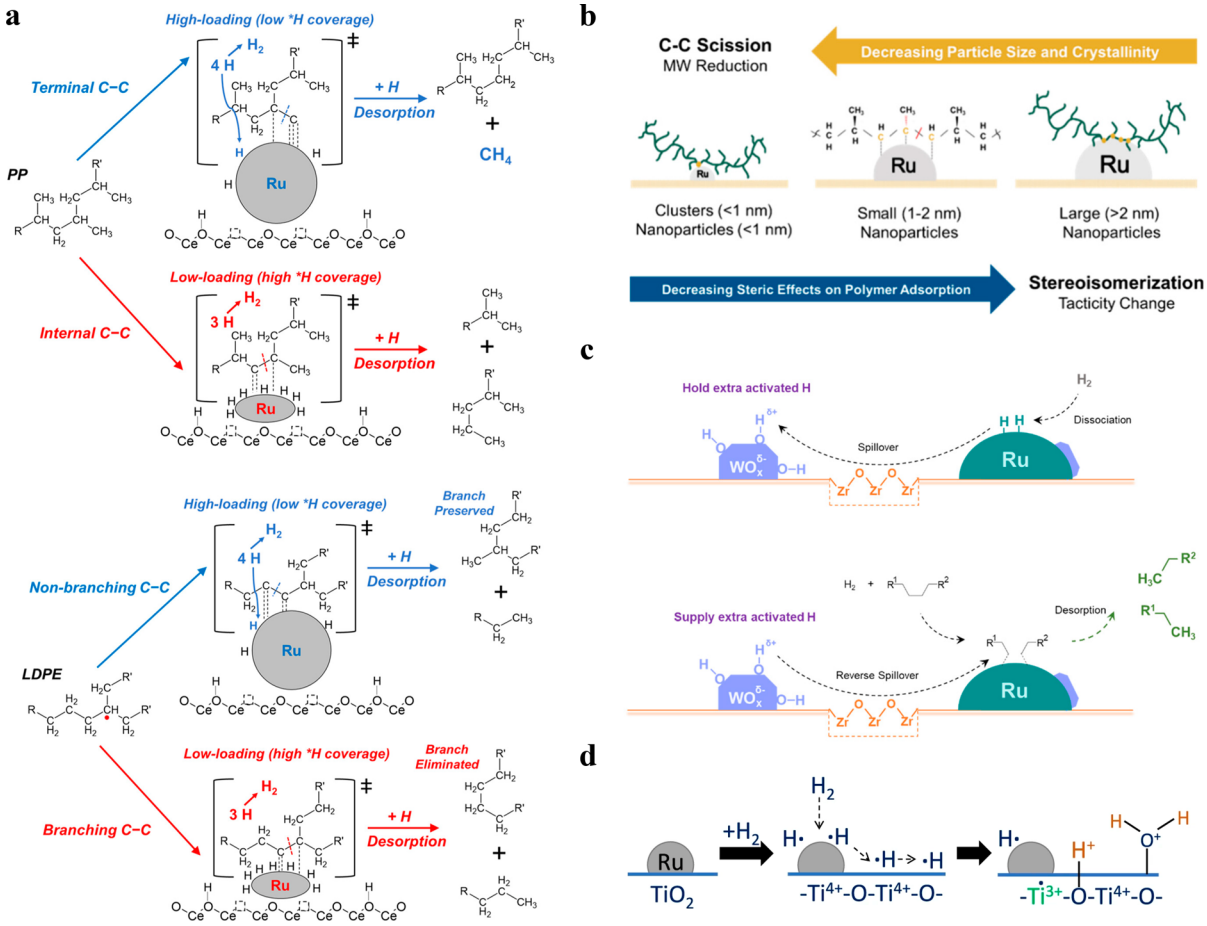

Figure 6. Effects of particle size and hydrogen spillover on PO hydrogenolysis. (a) Top panel shows (with PP as an example) that the higher *H coverage on low-loading Ru/CeO_2 favors internal over terminal C−C bond cleavage. Bottom panel shows that with LDPE as the substrate, the higher *H coverage on low-loading Ru/CeO_2 favors branching over nonbranching C−C bond cleavage. Reproduced with permission from ref 46. Copyright 2022 American Chemical Society. (b) Depiction of particle size effect on Ru/C *i*PP Hydrogenolysis Mechanism. Reproduced with permission from ref 49. Copyright 2024 American Chemical Society. (c) Selective pathway promoted by H_2 spillover and reverse spillover on Ru-WZr catalysts induced by ∼1 nm, slightly reduced $(WO_x)_n$ clusters. Reproduced with permission from ref 54. Available under a CC-BY-NC-ND 4.0 license. Copyright 2021 Cong Wang et al. (d) H_2 spillover schematic over Ru/TiO_2. Reproduced with permission from ref 57. Available under a CC-BY license. Copyright 2022 Pavel A. Kots et al.

materials. Advanced control in catalyst synthesis is essential to achieve the intended spatial arrangement of discrete architectural components. This necessitates the development of specialized synthetic methodologies for the precise placement of interactive catalytic sites, either similar or diverse, at defined distances and orientations from each other. Another level of cooperativity is combining C−C cleavage with a secondary process to create new conversion pathways. A successful example is one-pot hydrogenolysis/hydrocracking−aromatization of PE waste catalyzed by Pt/γ-Al_2O_3.[21] This process is self-sustaining as the hydrogen produced in the aromatization is enough to drive the C−C cleavage, eliminating the need for external hydrogen supplies and generating valuable long-alkyl-chain-functionalized aromatics.

CATALYSTS WITH WELL-DEFINED NANOSCOPIC STRUCTURES

As mentioned above, catalytic hydrogenolysis is generally regarded as a promising method that can convert end-of-life PO to value-added products, thus achieving the objectives of chemical upcycling and building a bright path to an environment-friendly and circular plastic economy. However, the severe methanation of PO on subnanometer metal clusters caused by favorable terminal C−C bond cleavages and fragmentation remained significant challenges. To overcome these challenges, researchers are focusing on nanoscale size control of active metals, polymer−support interaction, optimization of catalytic conditions (lower reaction temperatures and higher H_2 pressures), and the choice of special supports that can store H_2 on the reducible surface for H_2 spillover and reverse spillover, effectively desorb intermediate hydrocarbon chains, and thus suppress the yield of methane.

The Effects of Particle Size

Multiple active sites, including Ru, Pt, Ni, Co, and other elements, have been explored for PO hydrogenolysis. Among these elements, Ru and Pt are the most active d-metals for C−C bond cleavages and have received widespread attention and development. Recently, strontium-titanate-supported Pt (Pt/$SrTiO_3$) was reported to preferentially cleave long PE chains to high-quality liquid products with a small yield of volatile products in PE hydrogenolysis.[39] As the size of Pt NPs decreased, the yield of gas products increased, and the catalytic rate increased simultaneously, a feature for a structure-sensitive reaction. The yield of short products (C_1−C_6) from chain-end

https://doi.org/10.1021/jacsau.4c00289
JACS Au 2024, 4, 2081−2098

C−C bond cleavages was directly proportional to the conversion of longer polymer chains to short ones with more chain ends. Commercial Ru/C catalysts also behave in this manner, generating an increasing amount of gaseous products as the conversion increases in the hydrogenolysis of *n*-octadecane.[40−42] Hence, a thorough understanding of catalyst structural effects on product selectivity is crucial for enhancing catalytic hydrogenolysis performance. As illustrated above, in the catalytic system of $mSiO_2/Pt/SiO_2$, the size of Pt NPs significantly influenced the C−C bond cleavage rates.[35] Compared with large Pt NPs, smaller ones showed a faster rate of PE hydrogenolysis, revealing that PE hydrogenolysis rates increased with a more significant fraction of corner and edge sites than facet sites on Pt NPs. It can be inferred that hydrogenolysis catalyzed by $mSiO_2/Pt/SiO_2$ was also structure-sensitive, consistent with $Pt/SrTiO_3$. This trend was also observed in the hydrogenolysis of ethane catalyzed by Pt/SBA-15, where the TOF of 1.7 nm Pt was twice that of 2.9 nm Pt NPs.[43] Thus, the finding of smaller NPs associated with more rapid hydrogenolysis reactions is consistent for Pt NPs supported on silica as well as on $SrTiO_3$. An opposite trend has also been observed, in which smaller NPs on other supports give lower activity compared to larger NPs, such as Pt/Al_2O_3.[44]

Ru/ZrO_2 serves as another case where the TOF in LDPE hydrogenolysis increases from ca. 300 to 1200 h^{-1} as the particle size increases from ca. 1 to 9 nm.[45] Meanwhile, the Ru dispersion decreases as the particle size increases. These two factors lead to the conversion for LDPE hydrogenolysis increasing first and then decreasing with increasing Ru particle size at the same Ru/polymer ratio, showing a volcano plot with the highest conversion achieved at a particle size of 2.5 nm. To explore the reasonable explanations, active sites of Ru NPs were divided into edge, corner, and facet sites. The adsorption of PE on Ru facet sites is enhanced due to multipoint interaction between these sites and PE, which leads to the increase in TOF as the particle size increases. However, this strong adsorption of PE causes the production of gas products induced by consecutive hydrogenolysis. A different trend occurred on Ru/CeO_2.[46] At lower loadings with subnanometer clusters (<0.5 wt %), the intrinsic activity of Ru in the hydrogenolysis of PP increased as the particle size decreased, a trend inversely mirrored at higher loadings (>0.5 wt %). When transitioning into the low-loading range, Ru NPs were more cationic and highly disordered. The reports in small alkane hydrogenolysis show that electron-deficient Ru is less active in C−C bond hydrogenolysis,[47,48] opposite to the higher intrinsic activity with more cationic Ru in PO hydrogenolysis catalyzed by the low-loading Ru/CeO_2. The intriguing catalytic performance of low-loading Ru/CeO_2 is attributed to the highly disordered Ru species. Other than the impact on the activity, the disordered Ru species strengthens *H binding and increases surface *H coverage, leading to a lower ability to accommodate extra H from PE and thus favoring less-dehydrogenated transition states, such as internal C−C bond cleavage and branching C−C bond cleavage (Figure 6a). The size of metal NPs also affects the tacticity of liquid and solid products in the hydrogenolysis of isotactic polypropylene (*i*PP) catalyzed by Ru/C.[49] When the particle size decreases, the ratio of terrace sites decreases, which leads to a lower stereoisomerization rate (Figure 6b).

The Effects of Hydrogen Pressure

In addition to the effects of active sites, the regioselectivity of C−C bond cleavages can be modulated by varying H_2 pressure. For Ru/CeO_2, higher H_2 pressure favors the cleavages of internal C−C bonds, which suppress the formation of methane induced by terminal C−C cleavages.[46,50−52] Another study supports this conclusion by modeling hydrogenolysis reactions of squalene and alkanes.[52] The model reveals that the dissociation of $C_{tertiary}$−C bonds ($^3C-^XC$), terminal $C_{secondary}-C_{primary}$ bonds ($^2C-^1C$), and fragmentation exhibited negative reaction order in H_2 pressure.[53] In contrast, the dissociation of $C_{secondary}-C_{secondary}$ bonds ($^2C-^2C$) showed an approximately zero reaction order, supporting that a high H_2 pressure selectively favored the cleavages of $^2C-^2C$ bonds rather than $^2C-^1C$ and $^3C-^XC$ bonds. Chen et al. further proved this conclusion in the hydrogenolysis of PP and LDPE catalyzed by 0.125 and 2 wt % Ru/CeO_2.[46] They changed the H_2 pressure from 5 to 60 bar and found with H_2 pressure increases, CH_4 selectivity decreases due to the shift from cleaving terminal $^3C-^1C$ in PP and $^2C-^1C$ in LDPE to internal $^3C-^2C$ in PP and $^2C-^2C$ in LDPE. Interestingly, the selectivity of branched products reduces because of the regioselectivity shift from cleaving $^2C-^2C$ to $^3C-^2C$ bonds in LDPE. This H_2 pressure effect was also observed in PO hydrogenolysis catalyzed by Ru/C. When H_2 pressure increased from 5 to 75 bar, the PE conversion increased until 45 bar and then decreased due to a competition of active sites between PO and excess surface *H. Mechanistically, an important step of PO hydrogenolysis is dehydrogenation, which forms carbon−metal bonds and simultaneously weakens C−C bonds, leading to various dehydrogenated transition states. Higher H_2 pressure favors transition states with less dehydrogenation, which explains the observation that a rise in H_2 pressure favored the dissociation of internal over terminal C−C bonds and preferred branching C−C scissions to generate linear products.

The Effects of Hydrogen Spillover

Enhancing catalytic performance in PO hydrogenolysis can also be achieved by developing a reducible support surface that is capable of storing H_2 through hydrogen spillover from Ru.[54] This strategy was demonstrated on a Ru-$(WO_x)_n$-ZrO_2 catalyst. A notable issue with Ru/ZrO_2 is the strong binding of PE, which results in excessive overhydrogenolysis of strongly adsorbed intermediates and, thus, massive methane formation. Involving $(WO_x)_n$ clusters into this system suppressed methanation and shifted product distribution to heavier, more valuable paraffin because highly dispersed $(WO_x)_n$ clusters stored hydrogen in surface hydroxyls via hydrogen spillover from Ru that dissociated molecular H_2. During hydrogenolysis reaction on Ru, $(WO_x)_n$ clusters provided extra hydrogen to Ru through reverse spillover, promoting the rate-limiting hydrogenation/desorption processes, which occurred on the surface of Ru either by modifying catalyst−polymer interactions or by constructing new interfacial sites, thus efficiently removing reaction intermediates before their overhydrogenolysis (Figure 6c). Other intermediate reducible dopant oxides (V, Mo) play similar roles to $(WO_x)_n$, storing and supplying H_2 to Ru through spillover/reverse spillover to suppress the formation of methane.[55] Another promising support is partially reducible TiO_2.[56,57] A 3-fold increase in hydrogenolysis rates was achieved by modulating the reducibility of the TiO_2 support and strong metal−support

https://doi.org/10.1021/jacsau.4c00289
JACS Au 2024, 4, 2081−2098

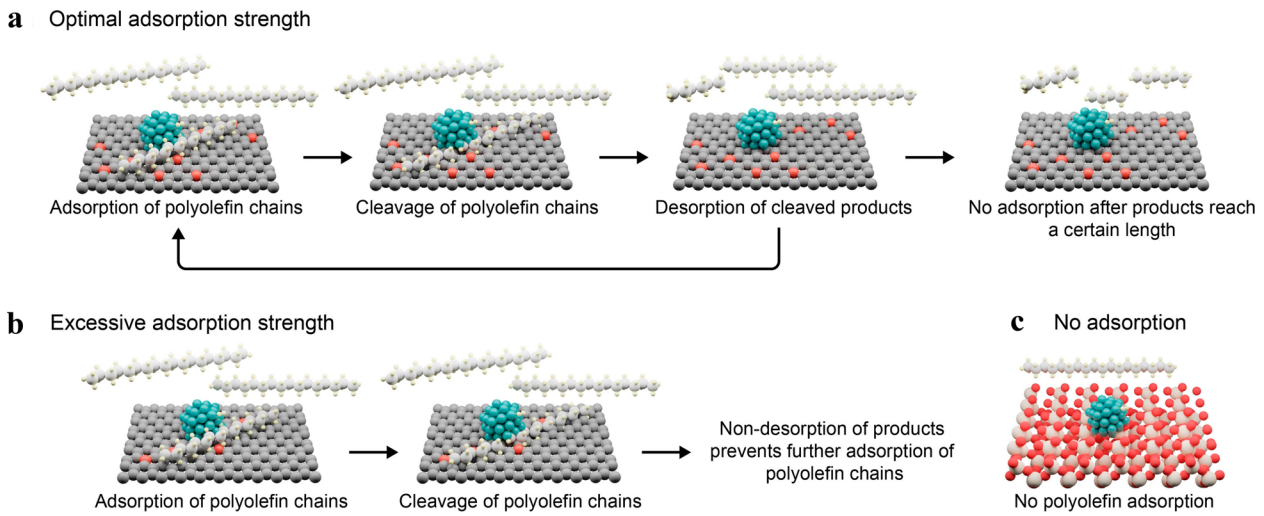

Figure 7. Effects of polymer−support interaction on PO hydrogenolysis. (a) Supports with optimal adsorption strength (Pt/AC1) do not further adsorb hydrocarbons and, therefore, limit the selectivity to a specific range of chain length. (b) Supports with excessive adsorption strength do not allow products to desorb and thus block the sites for further PP adsorption. (c) Supports that show no polymer adsorption do not promote contact of PP with Pt cleavage centers, resulting mostly in unconverted PP or residue. Reproduced with permission from ref 58. Copyright 2021Wiley-VCH GmbH.

interactions. The treatment of TiO_2 with ammonia (NH_3) enhanced hydrogen binding to Ru because of the H_2 spillover transferring from Ru to TiO_2, which formed delocalized electrons, reduced support more extensively, and increased the positive charges on Ru (Figure 6d). In other words, hydrogen storage capacity was boosted, promoting intermediates' desorption, preventing overhydrogenolysis, and increasing the liquid yield in PP hydrogenolysis. Thus, the capability of supplying hydrogen to active sites to hydrogenate and desorb hydrogenolysis products is a critical driver for enhancing catalytic performance, which represents a promising nanoscopic catalyst design strategy.

The Effects of Polymer−Support Interaction

Jaydev et al. demonstrated that carbon-supported Pt directly converted PP to motor oils (C_{21}−C_{45}) and explored the interaction between polymer chains and carbon supports.[58] The adsorption strength of hydrocarbons on the carbon support can be modulated by chain length and oxygen concentration doped on the support surface. Although they concluded that longer hydrocarbons possess stronger adsorption strength than shorter chains by comparing temperature-programmed desorption (TPD) results of linear alkanes (*n*-heptane, *n*-hexane, and *n*-pentane), this effect can hardly be practical in the design of catalysts. Therefore, they focused on oxygen-functionalized carbon supports and selected four activated carbon supports, i.e., AC, AC1, AC2, and AC3, with different surface oxygen concentrations, referencing SiO_2 and Al_2O_3. Compared with AC1, SiO_2 and Al_2O_3 show low *n*-heptane adsorption, indicating the poor adsorption capability of hydrocarbon on their surface. As a result, Pt/SiO_2 and Pt/Al_2O_3 display extremely low selectivity toward liquids, which proves the important role of adsorbing properties exhibited by carbon supports. Interestingly, AC with the lowest surface oxygen concentration among the four carbon supports is hardly able to desorb cracking products from AC and subsequently render the over cleavage of polymer chains to small alkanes, while AC1 with the highest surface oxygen concentration makes the desorption of certain-length hydrocarbons favorable and promotes the catalytic cycle. Another two carbon supports, AC2 and AC3, lie in between these two extreme situations. Additionally, AC1 has the highest cumulative micropore volume, which could also contribute to the observed support effect. To better understand the mechanism, they proposed three adsorption/desorption processes on different carbon supports (Figure 7). For supports with optimal adsorption strength, PP chains and intermediates can adsorb on the surface of supports and be cleaved at Pt sites until the hydrocarbon products are too small to stay adsorbed. However, for supports with excessive adsorption strength, it is difficult for PP chains and products to desorb, which hinders the adsorption of other polymer chains. Lastly, for supports that do not adsorb polymer chains, the rate of cleavage is much lower. In conclusion, controlling the interaction between polymer and support can drive the activity and selectivity of PP hydrogenolysis.

Polymer-porous support interaction can also induce the entropy confinement effect on PO hydrogenolysis.[59] High entropy is one of the intrinsic natures of PO, while the transition state decreases the entropy owing to the restriction of chain mobility, which results in unfavorable PO adsorption on catalysts and an unstable transition state. To overcome this challenge, Kang et al. used SBA-15 with mesoporous channels as the support and a precise impregnation method to make Ru NPs uniformly distributed inside the mesopores (p-Ru/SBA-15). SBA-15 with 9.1 nm pore diameter enables the balance between the space confinement effect and diffusion of PO chains. For comparisons, they prepared Ru/SiO_2 with Ru NPs supported on the surface of nonporous silica and c-Ru/SBA-15 by using the conventional impregnation method with Ru NPs located at both the internal and external surface of SBA-15. With Ru NPs of similar geometric and electronic features, p-Ru/SBA-15 exhibits better hydrogenolysis performance. Under the same reaction condition, the LDPE solid conversion on p-Ru/SBA-15 is 89.20%, whereas the conversions on c-Ru/SBA-15 and Ru/SiO_2 are 44.06% and 22.48%, respectively. However, these catalysts display similar product distributions when they maintain a consistent solid conversion of around 55% by regulating reaction time. These results demonstrate

https://doi.org/10.1021/jacsau.4c00289
JACS Au 2024, 4, 2081−2098

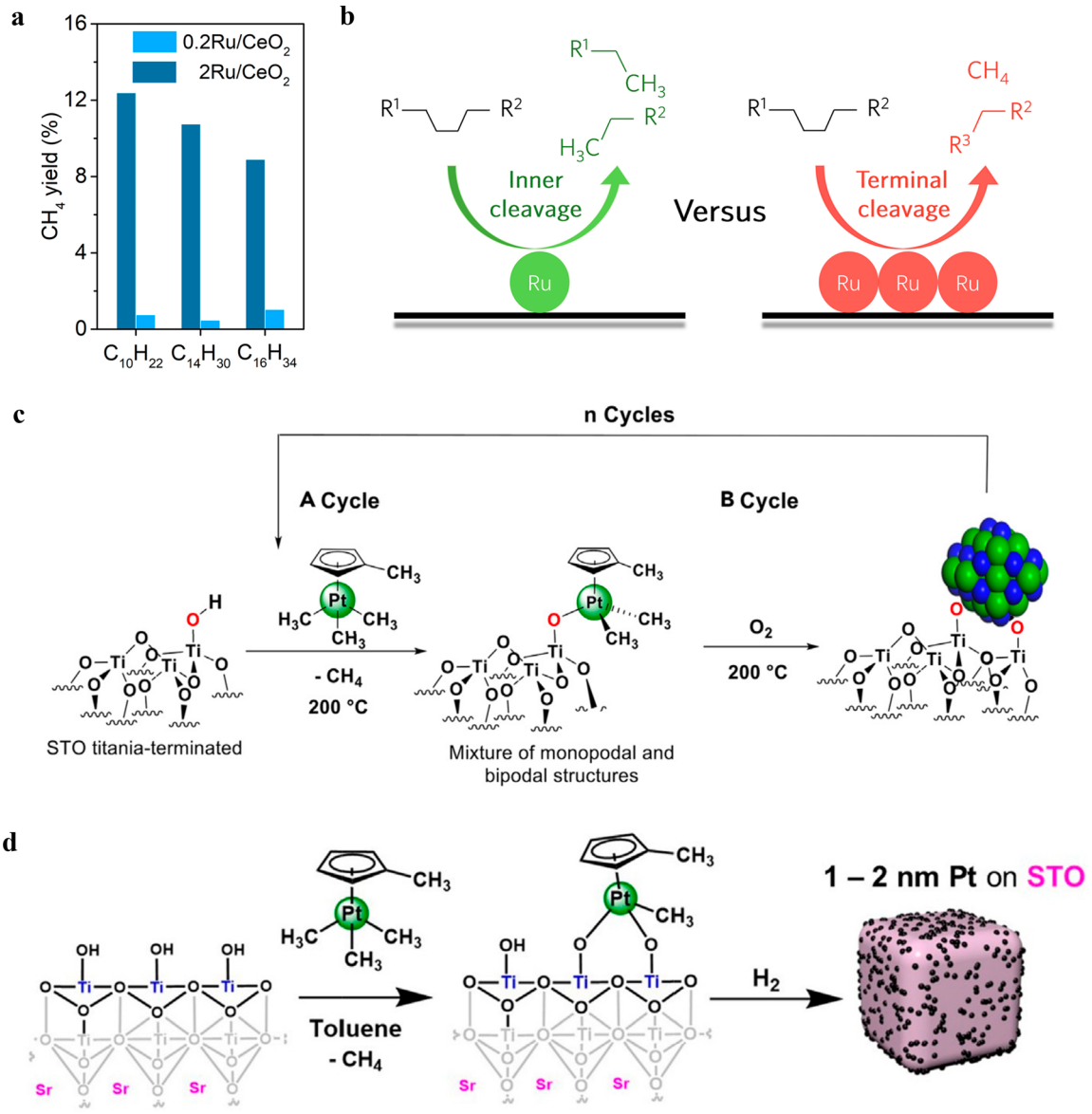

Figure 8. (a) Mechanism study of Ru SAC for PE hydrogenolysis. CH_4 yields in hydrogenolysis of alkanes with different chain lengths on Ru SAC and $2Ru/CeO_2$. Reaction conditions: T = 250 °C, P_{H2} = 2 MPa, t = 3 h, stirring rate = 400 rpm, and m(Ru)/m(alkane) = 1 mg/2,000 mg. (b) Summarized cleavage modes of PO on conventional SAC and nanocluster catalyst. (a) and (b) were reproduced with permission from ref 60. Available under a CC-BY-4.0 license. Copyright 2023 Mingyu Chu et al. (c) Representation of Pt/STO synthesis by ALD. In ALD, a cycle (A) is first employed to decorate the STO surface with a $MePtCpMe_3$ precursor, after which a cycle (B) is employed to anneal away the ligands and afford bare Pt NPs on STO. Reproduced with permission from ref 25. Copyright 2023 Elsevier Inc. (d) Schematic of SOMC-derived Pt/STO synthesis using a $MeCpPtMe_3$ precursor. Reproduced with permission from ref 62. Copyright 2023 Royal Society of Chemistry.

that the precise location of Ru NPs inside the mesoporous channels can enhance catalytic activity but exhibit negligible effects on product selectivity. ^{13}C MAS NMR further elucidates the entropy confinement effect on polymer chain freedom in SBA-15 channels by using *n*-eicosane as the model compound and observing the chemical shift of CH_2 and CH peaks located at 34.3 and 25.9 ppm, respectively. With the same ratio of catalyst/*n*-eicosane, p-Ru/SBA-15 shows more chemical shifts of CH_2 and CH to the high field, indicating SBA-15 support has a stronger interaction with *n*-eicosane than nonporous SiO_2. Therefore, the adsorption of LDPE chains in mesopores is more stable and efficiently decreases the entropy of these long polymer chains. Combined with thermodynamic analysis, the turnover rate depends on the difference in entropy before and after the adsorption of polymer reactants, $S^{\dagger} - S_{RH}$. Since the value of $S^{\dagger} - S_{RH}$ is negative, the less negative the value, the smaller the positive value of $-T\Delta S^{\dagger}$, lower activation free energy, and increasing catalytic activity.

Perspectives

Optimizing the size of active sites, polymer−support interaction, reaction conditions (including temperature and hydrogen pressure), and supports that allow hydrogen spillover/reverse spillover has shown initial success in suppressing methane formation and enhancing catalyst activity, selectivity, and stability in hydrogenolysis reactions. More studies are still necessary to further illustrate the mechanism and design principles of superior catalysts for hydrogenolysis. Although high hydrogen pressure can alleviate methane yield, it is not an ideal choice for practical applications, considering

https://doi.org/10.1021/jacsau.4c00289
JACS Au 2024, 4, 2081−2098

the high cost of instrumentation and operation. Therefore, there is a strong need to develop catalysts that can suppress methane formation at low H_2 pressures. Compared with the modulation of reaction conditions, particle size is an important and feasible parameter that influences the rate of C−C scission and the tacticity of liquid and solid products. The optimal polymer−support interaction can also be modulated by different surface oxygen concentrations. The excessive interactions prohibit the desorption of products and block sites for polymer adsorption, while weak interaction results in negligible adsorption of polymer chains and C−C scission. Notably, polymer−porous-support interaction also leads to the entropy confinement effect, which can reach lower activation energy and higher catalytic activity by precisely impregnating metal NPs in mesopores. In addition, precious metals, such as Pt and Ru, are highly active for hydrogenolysis, but they are expensive and sporadic, leading to much higher expenses than earth-abundant elements, such as iron (Fe), cobalt (Co), nickel (Ni), and copper (Cu). It is an important research direction to partially or totally replace rare and expensive elements with inexpensive crustal elements that can maintain or exceed the performance of precious metals. The preparation of Pt- or Ru-based alloys could be a promising future direction. The involvement of an inexpensive secondary element could mitigate the adsorption strength of hydrogen and hydrogenolysis intermediates and prevent overhydrogenolysis to methane. Furthermore, the involvement of WO_x and partially reducible support, e.g., TiO_2, provides more possibilities in choosing superior supports for promising designs of hydrogenolysis catalysts. In the reported Ru-$(WO_x)_n$-ZrO_2 catalyst, the Ru and $(WO_x)_n$ on ZrO_2 support are randomly distributed, where a controlled placement of these two functional sites could lead to a uniform hydrogen spillover and reverse spillover, further enhancing the performance of the catalyst.

CATALYSTS WITH WELL-DEFINED STRUCTURES AT THE ATOMIC SCALE

During polymer deconstruction, methanation typically results from terminal C−C bond cleavages. Initially, limited chain ends yield minimal methane, but the growing number of chain ends with C−C bond cleavages inevitably yield much more methane as the reaction proceeds. Considering the experimental and theoretical results and future directions discussed in the part of the nanoscopic scale, although lowering the reaction temperature and increasing H_2 pressure can kinetically alleviate methane generation, these strategies are impractical due to the prolonged reaction time and costly equipment. Instead, optimizing the geometric configuration of active sites and catalyst architectures at the atomic level could further boost their catalytic activity and selectivity.

The Involvement of Single Metal Atom Sites

Compared to single sites, multisite metal NPs enable the cracking of adjacent C−C bonds of polymer chains, generating methane.[60] To overcome this challenge, lowering the energy barrier for cleaving internal C−C bonds and minimizing the adsorption of polymer chains on multisite metal NPs are promising strategies. Therefore, the involvement of a Ru single-atom catalyst (Ru SAC) provides a promising solution because isolated Ru atoms determine the type of C−C bond cleavages. Moreover, the strong interaction between Ru single atoms and CeO_2 support not only ensures the uniform Ru atom dispersion but also prevents the leaching and aggregation of Ru, thus boosting catalyst stability. Compared to Ru NPs, this Ru SAC decreases methane yield from 21.1% to 2.2% and exhibits 94.5% liquid products. The mechanism behind this catalysis reveals that Ru single sites preferentially cleave internal C−C bonds, contrasting with multisite Ru NP catalysts that cannot prevent cleavage of terminal C−C bonds, which is further supported by hydrogenolysis reactions of model alkanes (Figure 8a−b). This single-site system demonstrates outstanding efficiency and versatility in PO hydrogenolysis, which shows a pronounced potential for industrial applications and merits more studies and extensions.

The Interaction between the Lattice-Matched Pt and $SrTiO_3$

Pt NPs supported on $SrTiO_3$ (Pt/STO) is another example showing the atomic level regulation of hydrogenolysis catalyst since the matched lattice between FCC Pt and STO nanocuboids surface leads to a strong metal−support interaction, which can prevent Pt NPs from leaching or sintering during catalytic reactions.[25,39,61,62] Atomic layer deposition (ALD) was used to prepare Pt/STO, realizing the uniform deposition of Pt NPs.[39] The loading, size, and edge-to-facet ratio of Pt NPs can be effectively controlled via increasing/decreasing the number of ALD cycles (Figure 8c). In this sense, 1c-, 5c-, and 10c-Pt/STO were prepared, and the size of Pt NPs increased with more ALD cycles. By comparing the catalytic behaviors of these three catalysts, it was found that smaller Pt NPs with a high edge-to-face ratio led to the overhydrogenolysis of PE to form undesirable light-gaseous products. Considering the conversion rate and distribution of high-quality liquid products, 5c-Pt/STO was used as a primary catalyst, which converted PE to high-quality liquid products (M_n = 590 Da, M_w = 625 Da) with a low $Đ$ of 1.1. Intriguingly, similar catalysis results were observed in the hydrogenolysis reactions of PE with varying molecular weights. To investigate the mechanism behind PE hydrogenolysis catalyzed by Pt/STO, PE−catalyst interaction and structure sensitivities caused by varying sizes of Pt NPs were investigated. ^{13}C MAS NMR and computational modeling proved that PE chains were preferentially adsorbed on Pt NPs over the STO surface and longer polymer chains exhibited stronger binding on cleavage sites than shorter hydrocarbon chains. Furthermore, the density functional theory (DFT) calculations revealed that the irregularities on the Pt/STO surface induced by Pt NPs disfavored the all-anti conformation of PE chains. Among different types of Pt sites, Pt(100) sites were responsible for the adsorption of H atoms, while Pt(111) sites realized the adsorption and cleavages of hydrocarbon chains. In contrast to commercial Pt/Al_2O_3, Pt NPs have stronger interactions with STO rather than γ-Al_2O_3 support, leading to better catalytic stability. Therefore, it is a promising approach to boost the metal nanoparticle-support interactions by choosing atomic lattice-matched metal NPs and supports in catalyst preparation.

An alternative method, surface-organometallic chemistry (SOMC), has emerged as a viable solution-phase metal deposition method to synthesize Pt/STO, maintaining the advantages of ALD.[62] In this approach, Pt/STO catalysts are prepared on a gram scale by suspending STO supports in a solution of platinum acetylacetonate ($Pt(acac)_2$) or trimethyl(methylcyclopentadienyl)platinum(IV) ($MeCpPtMe_3$) in toluene under heating, followed by treating the ligated samples under hydrogen gas (H_2). This technique was employed over

https://doi.org/10.1021/jacsau.4c00289
JACS Au 2024, 4, 2081−2098

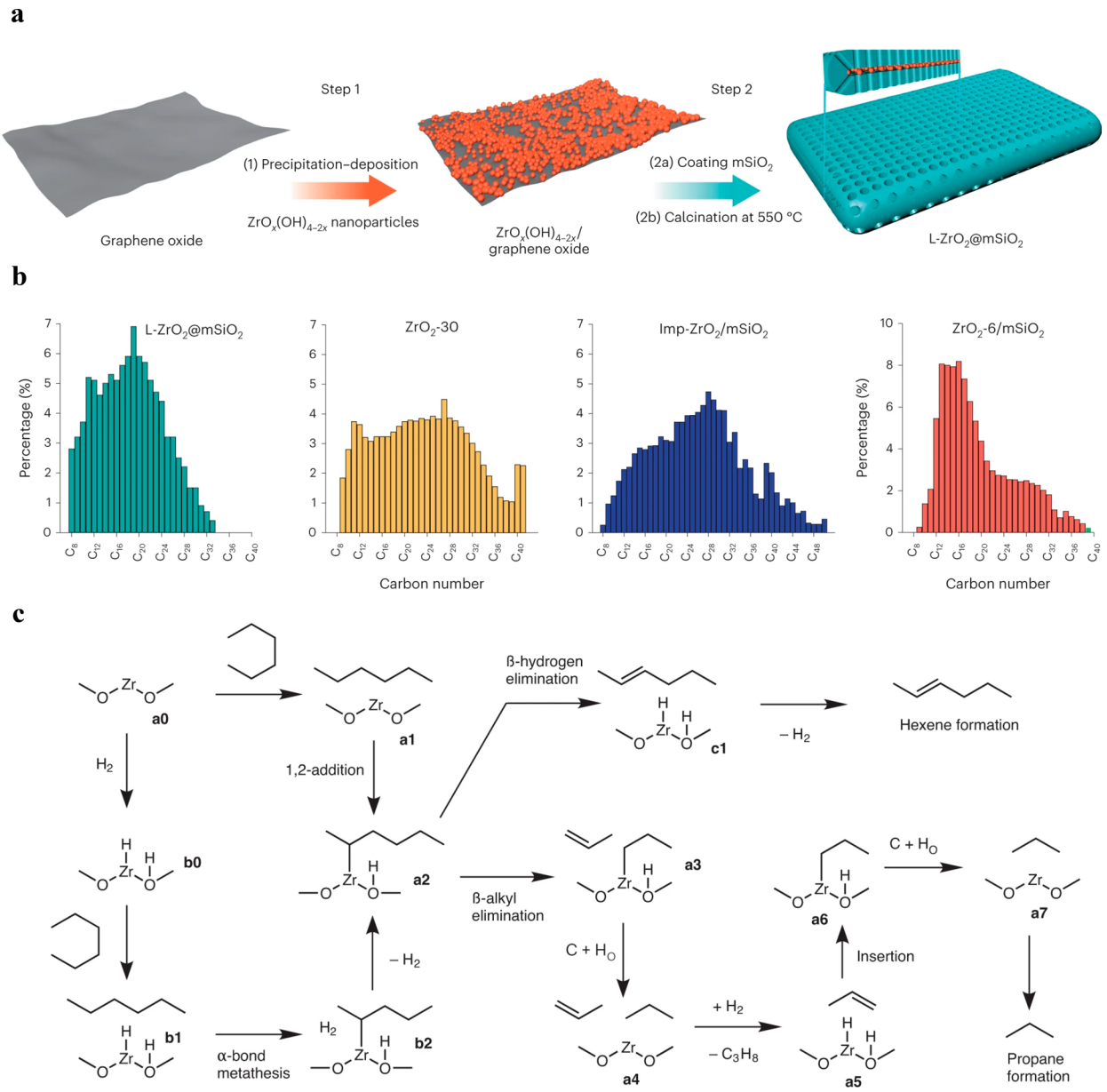

Figure 9. Involvement of earth-abundant ZrO_2 in the hydrogenolysis of PO. (a) Construction of L-ZrO_2@$mSiO_2$. (b) Hydrogenolysis results from L-ZrO_2@$mSiO_2$ and control catalysts. Carbon number distribution of liquid products catalyzed by L-ZrO_2@$mSiO_2$, ZrO_2-30 (30 nm particle diameter), Imp-ZrO_2/$mSiO_2$ (with randomly distributed ZrO_2 particles prepared by impregnation), and ZrO_2-6/$mSiO_2$ (6 nm particle diameter), obtained from reactions that consumed similar moles of H_2. (c) Calculated mechanistic model for hydrocarbon hydrogenolysis. Schematic of the reaction pathways considered for *n*-hexane hydrogenolysis on the $Zr(O)_2$/m-ZrO_2 and H–Zr(O)(OH)/m-ZrO_2 models. Reproduced with permission from ref 66. Available under a CC-BY license. Copyright 2023 Shaojiang Chen et al.

three consecutive cycles of deposition and reduction, leading to the formation of Pt NPs with average sizes ranging from 1.2 to 1.8 nm, which depends on the specific conditions used. SOMC-derived Pt/STO was successfully applied in upcycling *i*PP with a starting M_n of 5000 Da into liquid products having an average M_n of 270 Da and $Đ$ of 1.1. This performance was replicated even after five successive hydrogenolysis runs. Notably, the average diameter of the Pt NPs remained consistent (1.3 ± 0.3, 1.2 ± 0.39, 1.5 ± 0.35 nm) across various SOMC deposition cycles. It indicates a distinctive cycle-by-cycle growth behavior in SOMC under reducing conditions, differing from ALD, where oxidizing conditions typically facilitate particle growth rather than initiating new nucleation in subsequent cycles. Strong electrostatic adsorption (SEA) is another promising technique to deposit Pt on STO.[61] Under equivalent reaction conditions, the catalysts derived from ALD, SOMC, and SEA produced similar products, verified by GPC and NMR.[25]

The Study of Zirconium Hydride in PO Hydrogenolysis

Since noble metals are expensive and rare, replacing noble elements with inexpensive and earth-abundant elements is worth further exploration and development. Dufaud and Basset reported the application of earth-abundant zirconium (Zr) hydride in PO hydrogenolysis under milder temperatures (<150 °C) and atmospheric pressure.[63] The well-defined catalyst zirconium hydride supported on silica $(\equiv SiO)_3ZrH$ can be synthesized by surface organometallic chemical reactions, in which the zirconium center is electrophilic,

https://doi.org/10.1021/jacsau.4c00289
JACS Au 2024, 4, 2081−2098

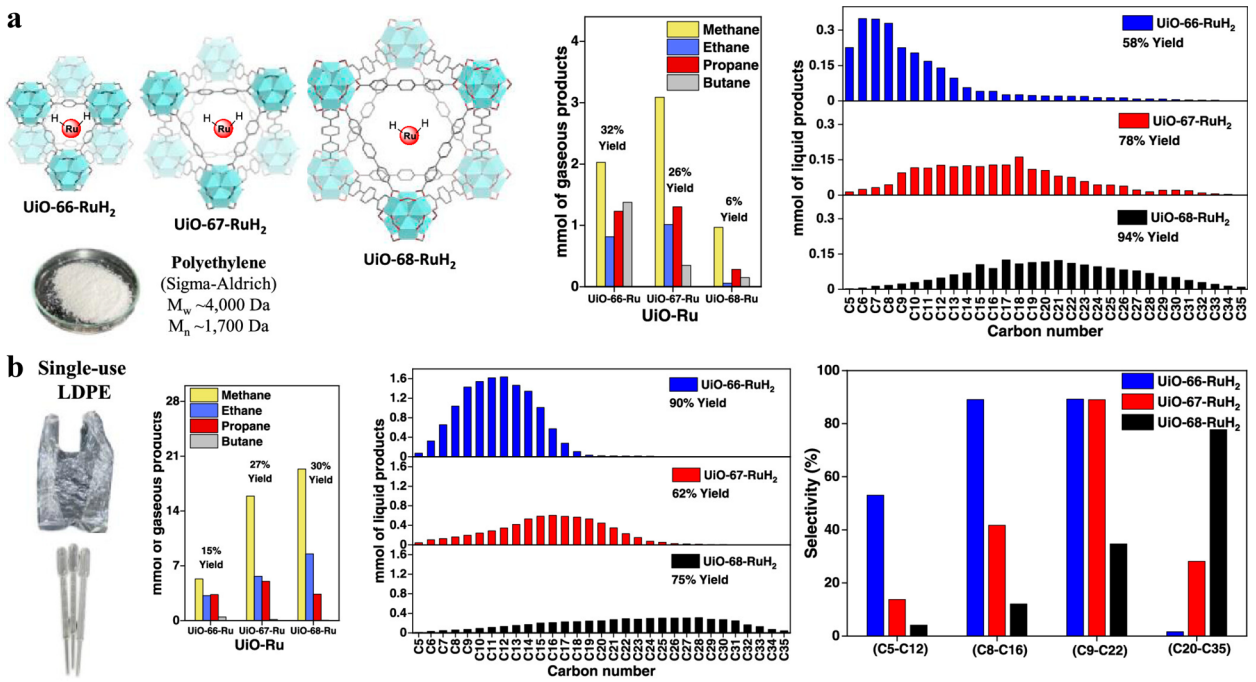

Figure 10. Catalytic performance of MOF-supported Ru dihydride in PO hydrogenolysis. (a) Hydrogenolysis of commercially available PE by UiO-Ru of different pore sizes to afford liquid and gaseous products. Reaction conditions: 0.60 g of polymer substrate, ~4 μmol of Ru, 200 °C, 35 bar H_2, and 72 h. (b) Hydrogenolysis of postconsumer single-use LDPE plastic bags or droppers by UiO-Ru of different pore sizes to afford liquid and gaseous products along with % selectivity of liquid products in several alkane ranges. Reaction conditions: 2.4 g of polymer substrate, ~16 μmol of Ru, 200 °C, 35 bar H_2, and 20 h. Reproduced with permission from ref 67. Available under a CC-BY-NC-ND 4.0 license. Copyright 2023 Manav Chauhan et al.

promoting the activation of C−H bonds and the cleavage of C−C bonds in alkanes. Since the backbones of PO possess analogous hydrocarbon chains as in higher alkanes, the catalytic C−C bond cleavage in PO can also be catalyzed by silica-supported $[Zr]_s$−H or even more electrophilic silica−alumina-supported $[Zr]_s$−H. The alumina hydride groups are located close to the Zr center, which makes it more electrophilic and thus enhances the catalytic performance in PO hydrogenolysis.[64] Norsic et al. further explored the different catalytic performances between groups 4, 5, and 6 metal hydrides (M = Zr, Hf, Ta, W) supported on silica−alumina.[65] In the hydrogenolysis reactions of alkane waxes, they found that supported $[Zr]_s$−H exhibits the highest catalytic activity, which shows that metal hydrides in group 4 are promising to improve the catalytic performance of PO hydrogenolysis.

The Application of Earth-Abundant ZrO_2

Even though Zr hydride shows promising activity in the catalytic hydrogenolysis of PO, the air- and water-sensitive nature of Zr−H hinders its application. On the other hand, Chen et al. demonstrated that the oxygen- and water-stable ZrO_2 can be easily prepared and integrated into silica-based porous structures with $Zr(O)_2$ adatom serving as the active site for C−C cleavage.[66] To realize this design, a metal oxide-mesoporous silica architecture was constructed by depositing ultrasmall $ZrO_x(OH)_{4-2x}$ NPs on the surface of single-layer graphene oxides and then growing $mSiO_2$ shells outside to form $mSiO_2/ZrO_x(OH)_{4-2x}$/graphene oxide structures. To create a more open catalytic architecture, graphene oxide was removed by calcination. Thus, amorphous localized ZrO_2 NPs (L-ZrO_2) were embedded into mesoporous silica to construct L-ZrO_2@$mSiO_2$ (Figure 9a), in which the ultrasmall L-ZrO_2 NPs were confined in the narrow zone between two $mSiO_2$ platelets. The presence of silica and the strong interaction between ZrO_2 and SiO_2 limit the crystallization and growth of L-ZrO_2. L-ZrO_2@$mSiO_2$ represents another promising "open−open" architecture discussed in the mesoscopic section with defined pore diameter, pore length, and location of active sites, which can be adapted in synthesizing well-defined catalysts using precious elements, inexpensive elements, and metal oxides as the active sites. L-ZrO_2@$mSiO_2$-catalyzed hydrogenolysis of PE leads to a narrower, Gaussian C_{18}-centered alkane product distribution, while other ZrO_2 control catalysts gave broad, non-Gaussian product distribution (Figure 9b). In addition, the ultrasmall amorphous ZrO_2 NPs contain more active sites than larger crystalline ZrO_2 NPs normalized by mass, agreeing with the predicted $Zr(O)_2$ adatom active sites that are more likely to present on unsaturated amorphous ZrO_2 surface. The C−C cleavage mechanism on L-ZrO_2@$mSiO_2$ varied from those reported for metal NPs, reducible oxides, and even SOMC Zr hydride. DFT calculations suggest the heterolytic cleavages of H−H and C−H bonds on adatom $Zr(O)_2/ZrO_2$ generate O−H and Zr−H or Zr−CH_2CH_2R species and subsequently engage in protonolytic elimination, insertion, and β-alkyl elimination (Figure 9c). The adatom $Zr(O)_2/ZrO_2$ active sites have a much better air- and water-stability than organometallic Zr−H active sites.

MOF-Supported Ru Dihydride in PO Hydrogenolysis

Three ordered zirconium UiO-metal−organic frameworks (UiO-MOFs)-supported Ru dihydrides (UiO-RuH_2) catalysts, UiO-66-RuH_2, UiO-67-RuH_2, and UiO-68-RuH_2 with pore sizes of 5.1, 6.8, 8.1 Å, were synthesized to catalyze PO hydrogenolysis reactions.[67] The product distributions from hydrogenolysis of PE (M_n: ~1700 Da, M_w: ~4000 Da),

https://doi.org/10.1021/jacsau.4c00289
JACS Au 2024, 4, 2081−2098

depicted in Figure 10a, showed a noticeable shift from lighter, narrower to heavier, broader when the MOF pore sizes are increased from 5.1 to 8.1 Å. Although methane was always the dominant component in gaseous products regardless of the pore size of MOFs, UiO-68-RuH_2 gave an excellent yield of 94% of liquid products. In addition to the hydrogenolysis of commercial PE, this series of catalysts is also applied to postconsumer single-use LPDE such as plastic bags and droppers (Figure 10b). Interestingly, a similar shift of product distributions with increasing pore size was observed, meaning the distribution of products can be tuned by the pore size of MOFs. The reusability tests show that UiO-RuH_2 could be recycled more than five times with an intact MOF structure and negligible leaching of Ru and Zr. In addition to the involvement of well-defined MOF structures, single atomic Ru sites also promoted the activation and cleavage of sterically encumbered internal C−C bonds in PE, suppressing methanation. The DFT calculation showed that β-alkyl transfer was the turnover-limiting step (TLS) due to the high activation barrier. This work demonstrated that superior catalytic performances were achieved by the combination of Ru single sites and well-defined MOF structures with tunable pore size and excellent stability.

Perspectives

PO hydrogenolysis by well-defined catalysts at the atomic scale is still in its infancy. More catalysts with single atomic sites need to be studied to realize the full potential of these atomic-level controlled catalysts, just like the observed transformation from terminal to internal C−C bond cleavages to suppress methane formation on the Ru/CeO_2 single-atom catalyst. Embedding single sites in enzyme-like architectures, well-defined MOF structures, zeolites, or partially reducible supports could enable combined benefits of both components in a catalytic system. As demonstrated that the MOF pore size in UiO-RuH_2 plays a significant role in controlling the hydrogenolysis product chain length, the large space in MOF pore geometry control has not been explored for PO hydrogenolysis. Another direction is the cooperation between lattice-matched active sites and supports, like the preparation of Pt/$SrTiO_3$, enabling the stabilization of Pt NPs on the surface of $SrTiO_3$ with negligible aggregations and leaching of Pt under hydrogenolysis reaction conditions. The successful epitaxial growth of PtO_2 atomic layers on rutile-type TiO_2 with similar lattice parameters was also reported recently, allowing the electronic state modulation of Pt species on rutile TiO_2 and achieving outstanding stability and activity in thermocatalytic and electrocatalytic reactions.[68] This rational design can also be applied to other metal active sites on oxide supports with matched or similar lattice constants, which provides a potential strategy for the synthesis of hydrogenolysis catalysts. In addition, compared with metal hydrides in groups 5 and 6, the metal hydrides in group 4 are more promising to improve the catalytic performance of PO hydrogenolysis, especially the earth-abundant Zr hydride. However, the primary challenge facing Zr-hydride-based catalysts lies in their susceptibility to water and oxygen. Therefore, preparing and precisely locating water- and air-stable Zr species into an appropriate architecture is the prerequisite for advancements in Zr-based catalysts.

CONCLUSIONS AND OUTLOOK

Creating structurally well-defined catalysts that can achieve desired selective deconstructions of PO is of paramount importance. After summarizing recent advancements in catalyst development focusing on mesoscale, nanoscopic, and atomic level structure control, numerous possibilities and opportunities are worth further exploring. Here, we divide these possible avenues into the following categories.

(1) The implementation of processivity and cooperativity from natural enzymes into the design of enzyme-mimic catalysts enables selective bond cleavage and functionalization. Processivity can be achieved by precisely positioning active sites, where bond-making or -cleaving occurs, in a porous architecture with atomic-level defined pores. The interaction between polymer and pore enables the whole polymer chain to be converted to uniform smaller products before desorbing from pores, thereby enhancing the catalytic efficiency and product selectivity in PO hydrogenolysis. Cooperativity can be attained by controlling the spatial arrangement of interactive catalytic sites at defined distances and orientations, which can combine the characteristics of diverse active sites in synthetic materials.

(2) The optimization of tunable porous structures with the ability to precisely position active sites, such as zeolites, MOFs, and COFs, can produce narrow and tunable PO hydrogenolysis products. The pore diameter is a pivotal parameter in designing well-defined porous catalysts, which determines the residence time of polymers near active sites, the conformation of polymer chains in the pore, and final product distribution. To achieve an atomic-level confined environment, crystalline zeolites, MOFs, and COFs are regarded as ideal selections. However, the slow product diffusion of polymer and products in microporous channels could be the main challenge, hindering the development of zeolite-support catalysts. Therefore, the study of accurately controlling the embedding depth of active sites below the surface of zeolites is important. In addition, maintaining superior stability of MOFs and COFs under hydrogenolysis reaction conditions is another future research direction.

(3) The selection of specific supports that can effectively adsorb long polymer chains, desorb the intermediates and products, stabilize the active sites, or cooperate with active sites. The supports with hydrogen storage capability can promote the rate-limiting hydrogenation/desorption step, which can efficiently desorb intermediates, prevent overhydrogenolysis, and suppress methanation during hydrogenolysis. Additionally, depositing metal active sites on supports with matched or similar lattice constants can boost the interactions between metal NPs and supports, which stabilizes the metal NPs on the support surface with negligible aggregations or leaching during PO hydrogenolysis reactions. In addition, the polymer−support interaction is another significant parameter that can be regulated by changing the surface heteroatom concentrations, driving the activity and selectivity in PO hydrogenolysis. The entropy confinement effect induced by porous supports thermodynamically decreases the hydrogenolysis activation energy of adsorbed polymer and promotes catalytic activity.

(4) The involvement of single-atom catalytic sites in mesoscopic or nanoscopic catalyst systems can merge the benefits of atomically defined active sites with

https://doi.org/10.1021/jacsau.4c00289
JACS Au 2024, 4, 2081−2098

mesoscopic or nanoscopic confined environments to enhance the activity and selectivity of PO hydrogenolysis. Well-defined single sites could preferentially break internal C−C bonds to enhance the selectivity of liquid products and suppress the methanation. Therefore, incorporating single sites into enzyme-like well-defined architecture, such as MOFs and zeolites, can bring more opportunities in PO hydrogenolysis. In addition, the replacement of monofunctional noble elements, partially or completely, with inexpensive elements or multicomponent active sites, such as bimetallic, intermetallic, and high-entropy alloys, represents another promising avenue in decreasing the cost and promoting performance for large-scale conversion of waste PO.

Combined, these opportunities bring fresh impetus to the development of PO hydrogenolysis. These catalyst design principles obtained for PO hydrogenolysis can also be applied in the deconstruction of other polymers, ultimately achieving chemical upcycling objectives to realize circularity in plastic lifecycles.

AUTHOR INFORMATION

Corresponding Author

Wenyu Huang − *Department of Chemistry, Iowa State University, Ames, Iowa 50011, United States; US Department of Energy, Ames National Laboratory, Ames, Iowa 50011, United States;* orcid.org/0000-0003-2327-7259; Email: whuang@iastate.edu

Author

Simin Sun − *Department of Chemistry, Iowa State University, Ames, Iowa 50011, United States; US Department of Energy, Ames National Laboratory, Ames, Iowa 50011, United States;* orcid.org/0000-0003-4171-3114

Complete contact information is available at: https://pubs.acs.org/10.1021/jacsau.4c00289

Notes

The authors declare no competing financial interest.

ACKNOWLEDGMENTS

This work was supported by the Institute for Cooperative Upcycling of Plastics (iCOUP), an Energy Frontier Research Center funded by the U.S. Department of Energy (DOE), Office of Basic Energy Sciences. Ames National Laboratory is operated by Iowa State University under Contract DE-AC-02-07CH11358.

REFERENCES

(1) Korley, L. T. J.; Epps, T. H.; Helms, B. A.; Ryan, A. J. Toward Polymer Upcycling—Adding Value and Tackling Circularity. *Science* **2021**, *373* (6550), 66−69.

(2) OECD. Executive Summary. In *Global Plastics Outlook: Economic Drivers, Environmental Impacts and Policy Options*; OECD Publishing: Paris, 2022. .

(3) Chu, M.; Liu, Y.; Lou, X.; Zhang, Q.; Chen, J. Rational Design of Chemical Catalysis for Plastic Recycling. *ACS Catal.* **2022**, *12* (8), 4659−4679.

(4) Kosloski-Oh, S. C.; Wood, Z. A.; Manjarrez, Y.; de los Rios, J. P.; Fieser, M. E. Catalytic Methods for Chemical Recycling or Upcycling of Commercial Polymers. *Mater. Horiz.* **2021**, *8* (4), 1084−1129.

(5) Chen, X.; Wang, Y.; Zhang, L. Recent Progress in the Chemical Upcycling of Plastic Wastes. *ChemSusChem* **2021**, *14* (19), 4137−4151.

(6) Tian, S.; Jiao, Y.; Gao, Z.; Xu, Y.; Fu, L.; Fu, H.; Zhou, W.; Hu, C.; Liu, G.; Wang, M.; et al. Catalytic Amination of Polylactic Acid to Alanine. *J. Am. Chem. Soc.* **2021**, *143* (40), 16358−16363.

(7) Zhang, M.-Q.; Wang, M.; Sun, B.; Hu, C.; Xiao, D.; Ma, D. Catalytic Strategies for Upvaluing Plastic Wastes. *Chem.* **2022**, *8* (11), 2912−2923.

(8) Cao, R.; Zhang, M.-Q.; Jiao, Y.; Li, Y.; Sun, B.; Xiao, D.; Wang, M.; Ma, D. Co-Upcycling of Polyvinyl Chloride and Polyesters. *Nat. Sustain.* **2023**, *6* (12), 1685−1692.

(9) Hu, Y.; Zhang, S.; Xu, J.; Liu, Y.; Yu, A.; Qian, J.; Xie, Y. Highly Efficient Depolymerization of Waste Polyesters Enabled by Transesterification/Hydrogenation Relay Under Mild Conditions. *Angew. Chem., Int. Ed.* **2023**, *62* (45), No. e202312564.

(10) Kots, P. A.; Vance, B. C.; Quinn, C. M.; Wang, C.; Vlachos, D. G. A Two-Stage Strategy for Upcycling Chlorine-Contaminated Plastic Waste. *Nat. Sustain.* **2023**, *6* (10), 1258−1267.

(11) Mark, L. O.; Cendejas, M. C.; Hermans, I. The Use of Heterogeneous Catalysis in the Chemical Valorization of Plastic Waste. *ChemSusChem* **2020**, *13* (22), 5808.

(12) Cao, R.; Zhang, M.-Q.; Hu, C.; Xiao, D.; Wang, M.; Ma, D. Catalytic Oxidation of Polystyrene to Aromatic Oxygenates Over a Graphitic Carbon Nitride Catalyst. *Nat. Commun.* **2022**, *13* (1), 4809.

(13) Plastics−the Fast Facts 2023. Plastics Europe. 2023. https://plasticseurope.org/knowledge-hub/plastics-the-fast-facts-2023/.

(14) Yeung, C. W.; Teo, J. Y.; Loh, X. J.; Lim, J. Y. Polyolefins and Polystyrene as Chemical Resources for a Sustainable Future: Challenges, Advances, and Prospects. *ACS Mater. Lett.* **2021**, *3* (12), 1660−1676.

(15) Kasar, P.; Sharma, D.; Ahmaruzzaman, M. Thermal and catalytic decomposition of waste plastics and its co-processing with petroleum residue through pyrolysis process. *J. Clean. Prod.* **2020**, *265*, No. 121639.

(16) Chu, M.; Tu, W.; Yang, S.; Zhang, C.; Li, Q.; Zhang, Q.; Chen, J. Sustainable chemical upcycling of waste polyolefins by heterogeneous catalysis. *SusMat* **2022**, *2* (2), 161−185.

(17) Ignatyev, I. A.; Thielemans, W.; Vander Beke, B. Recycling of Polymers: A Review. *ChemSusChem* **2014**, *7* (6), 1579−1593.

(18) Vollmer, I.; Jenks, M. J.; Mayorga González, R.; Meirer, F.; Weckhuysen, B. M. Plastic Waste Conversion over a Refinery Waste Catalyst. *Angew. Chem., Int. Ed.* **2021**, *60* (29), 16101−16108.

(19) Liu, S.; Kots, P. A.; Vance, B. C.; Danielson, A.; Vlachos, D. G. Plastic Waste to Fuels by Hydrocracking at Mild Conditions. *Sci. Adv.* **2021**, *7* (17), eabf8283.

(20) Hinton, Z. R.; Kots, P. A.; Soukaseum, M.; Vance, B. C.; Vlachos, D. G.; Epps, T. H.; Korley, L. T. Antioxidant-Induced Transformations of a Metal-Acid Hydrocracking Catalyst in the Deconstruction of Polyethylene Waste. *Green Chem.* **2022**, *24* (19), 7332−7339.

(21) Zhang, F.; Zeng, M.; Yappert, R. D.; Sun, J.; Lee, Y.-H.; LaPointe, A. M.; Peters, B.; Abu-Omar, M. M.; Scott, S. L. Polyethylene Upcycling to Long-Chain Alkylaromatics by Tandem Hydrogenolysis/Aromatization. *Science* **2020**, *370* (6515), 437−441.

(22) Wei, J.; Liu, J.; Zeng, W.; Dong, Z.; Song, J.; Liu, S.; Liu, G. Catalytic Hydroconversion Processes for Upcycling Plastic Waste to Fuels and Chemicals. *Catal. Sci. Technol.* **2023**, *13* (5), 1258−1280.

(23) Jaydev, S. D.; Martín, A. J.; Usteri, M.-E.; Chikri, K.; Eliasson, H.; Erni, R.; Pérez-Ramírez, J. Consumer Grade Polyethylene Recycling via Hydrogenolysis on Ultrafine Supported Ruthenium Nanoparticles. *Angew. Chem., Int. Ed.* **2024**, *63* (11), No. e202317526.

(24) Musa, A.; Jaseer, E.; Barman, S.; Garcia, N. Review on Catalytic Depolymerization of Polyolefin Waste by Hydrogenolysis: State-of-the-Art and Outlook. *Energy Fuels* **2024**, *38* (3), 1676−1691.

(25) Peczak, I. L.; Kennedy, R. M.; Hackler, R. A.; Lee, B.; Meirow, M.; Luijten, E.; Poeppelmeier, K. R.; Delferro, M. Treasuring Trash: Pt/$SrTiO_3$ Catalysts Process Plastic Waste into High-Value Materials. *Matter* **2023**, *6* (10), 3296−3321.

(26) Faust, K.; Denifl, P.; Hapke, M. Recent advances in catalytic chemical recycling of polyolefins. *ChemCatChem.* **2023**, *15* (13), No. e202300310.
(27) Kots, P. A.; Vance, B. C.; Vlachos, D. G. Polyolefin plastic waste hydroconversion to fuels, lubricants, and waxes: a comparative study. *React. Chem. Eng.* **2021**, *7* (1), 41−54.
(28) Koval, C. A.; Lercher, J.; Scott, S. L.; Coates, G. W.; Iglesia, E.; Bullock, R. M.; Jaramillo, T. F.; Flytzani-Stephanopoulos, M.; Resasco, D.; Tway, C. L. *Basic Research Needs for Catalysis Science to Transform Energy Technologies*. Report from the US Department of Energy, Office of Basic Energy Sciences Workshop May 8−10, 2017 in Gaithersburg, Maryland; *USDOE Office of Science (SC)(United States)*, 2017.
(29) van Dongen, S. F. M.; Elemans, J. A. A. W.; Rowan, A. E.; Nolte, R. J. M. Processive Catalysis. *Angew. Chem., Int. Ed.* **2014**, *53* (43), 11420−11428.
(30) Tennakoon, A.; Wu, X.; Paterson, A. L.; Patnaik, S.; Pei, Y.; LaPointe, A. M.; Ammal, S. C.; Hackler, R. A.; Heyden, A.; Slowing, I. I.; et al. Catalytic Upcycling of High-Density Polyethylene via a Processive Mechanism. *Nat. Catal.* **2020**, *3* (11), 893−901.
(31) Zhao, T. Y.; Meirow, M.; Tennakoon, A.; Wu, X.; Paterson, A. L.; Qi, L.; LaPointe, A. M.; Lamb, J. V.; Kobayashi, T.; Delferro, M.; et al. Mechanistic Insights into Processive Polyethylene Hydrogenolysis through In Situ NMR. *Macromolecules* **2023**, *56* (11), 4287−4295.
(32) Lyu, X.; Meirow, M.; Wu, X.; Zhou, X.; Liu, Y.; Huang, W.; Li, T.; Lee, B. Molecular-Weight-Dependent Infiltration and Adsorption of Polymers into Nanochannels. *ACS Appl. Mater. Interfaces* **2023**, *15* (22), 27369−27379.
(33) Yappert, R.; Peters, B. Processive Depolymerization Catalysts: A Population Balance Model for Chemistry's "While" Loop. *ACS Catal.* **2022**, *12*, 10353−10360.
(34) Du, J.; Zeng, L.; Yan, T.; Wang, C.; Wang, M.; Luo, L.; Wu, W.; Peng, Z.; Li, H.; Zeng, J. Efficient Solvent- and Hydrogen-Free Upcycling of High-Density Polyethylene into Separable Cyclic Hydrocarbons. *Nat. Nanotechnol.* **2023**, *18* (7), 772−779.
(35) Wu, X.; Tennakoon, A.; Yappert, R.; Esveld, M.; Ferrandon, M. S.; Hackler, R. A.; LaPointe, A. M.; Heyden, A.; Delferro, M.; Peters, B.; et al. Size-Controlled Nanoparticles Embedded in a Mesoporous Architecture Leading to Efficient and Selective Hydrogenolysis of Polyolefins. *J. Am. Chem. Soc.* **2022**, *144* (12), 5323−5334.
(36) Meirow, M.; Luijten, E. Coarse-Grained Modeling of Polymer Cleavage within a Porous Catalytic Support. *ACS Macro Lett.* **2023**, *12* (2), 189−194.
(37) Meirow, M.; Tennakoon, A.; Wu, X.; Willmon, J.; Howell, D.; Huang, W.; Sadow, A. D.; Luijten, E. Influence of Pore Length on Hydrogenolysis of Polyethylene within a Mesoporous Support Architecture. *J. Phys. Chem. C* **2023**, *127* (49), 23805−23813.
(38) Tennakoon, A.; Wu, X.; Meirow, M.; Howell, D.; Willmon, J.; Yu, J.; Lamb, J. V.; Delferro, M.; Luijten, E.; Huang, W.; et al. Two Mesoporous Domains Are Better Than One for Catalytic Deconstruction of Polyolefins. *J. Am. Chem. Soc.* **2023**, *145* (32), 17936−17944.
(39) Celik, G.; Kennedy, R. M.; Hackler, R. A.; Ferrandon, M.; Tennakoon, A.; Patnaik, S.; LaPointe, A. M.; Ammal, S. C.; Heyden, A.; Perras, F. A.; et al. Upcycling Single-Use Polyethylene into High-Quality Liquid Products. *ACS Cent. Sci.* **2019**, *5* (11), 1795−1803.
(40) Rorrer, J. E.; Beckham, G. T.; Román-Leshkov, Y. Conversion of Polyolefin Waste to Liquid Alkanes with Ru-Based Catalysts under Mild Conditions. *JACS Au* **2021**, *1* (1), 8−12.
(41) Rorrer, J. E.; Troyano-Valls, C.; Beckham, G. T.; Román-Leshkov, Y. Hydrogenolysis of Polypropylene and Mixed Polyolefin Plastic Waste over Ru/C to Produce Liquid Alkanes. *ACS Sustain. Chem. Eng.* **2021**, *9* (35), 11661−11666.
(42) Chen, L.; Zhu, Y.; Meyer, L. C.; Hale, L. V.; Le, T. T.; Karkamkar, A.; Lercher, J. A.; Gutiérrez, O. Y.; Szanyi, J. Effect of Reaction Conditions on the Hydrogenolysis of Polypropylene and Polyethylene into Gas and Liquid Alkanes. *React. Chem. Eng.* **2022**, *7*, 844−854.
(43) Song, H.; Rioux, R. M.; Hoefelmeyer, J. D.; Komor, R.; Niesz, K.; Grass, M.; Yang, P.; Somorjai, G. A. Hydrothermal Growth of Mesoporous SBA-15 Silica in the Presence of PVP-Stabilized Pt Nanoparticles: Synthesis, Characterization, and Catalytic Properties. *J. Am. Chem. Soc.* **2006**, *128* (9), 3027−3037.
(44) Le Valant, A.; Drault, F.; Maleix, C.; Comminges, C.; Beauchet, R.; Batonneau, Y.; Pirault-Roy, L.; Especel, C.; Epron, F. Effect of the Metallic Particle Size of Supported Pt Catalysts on Methylcyclopentane Hydrogenolysis: Understanding of the Ring Opening Products Distribution by a Geometric Approach. *J. Catal.* **2018**, *367*, 234−243.
(45) Tamura, M.; Miyaoka, S.; Nakaji, Y.; Tanji, M.; Kumagai, S.; Nakagawa, Y.; Yoshioka, T.; Tomishige, K. Structure-Activity Relationship in Hydrogenolysis of Polyolefins over Ru/Support Catalysts. *Appl. Catal., B* **2022**, *318*, No. 121870.
(46) Chen, L.; Meyer, L. C.; Kovarik, L.; Meira, D.; Pereira-Hernandez, X. I.; Shi, H.; Khivantsev, K.; Gutiérrez, O. Y.; Szanyi, J. Disordered, Sub-Nanometer Ru Structures on CeO_2 are Highly Efficient and Selective Catalysts in Polymer Upcycling by Hydrogenolysis. *ACS Catal.* **2022**, *12* (8), 4618−4627.
(47) Coq, B.; Bittar, A.; Dutartre, R.; Figueras, F. Influence of the Precursor and the Support on the Catalytic Properties of Ruthenium for Alkane Hydrogenolysis. *Appl. Catal.* **1990**, *60* (1), 33−46.
(48) Bond, G. C.; Coq, B.; Dutartre, R.; Ruiz, J. G.; Hooper, A. D.; Proietti, M. G.; Sierra, M. C. S.; Slaa, J. C. Effect of Various Pretreatments on the Structure and Properties of Ruthenium Catalysts. *J. Catal.* **1996**, *161* (1), 480−494.
(49) Sun, J. A.; Kots, P. A.; Hinton, Z. R.; Marinkovic, N. S.; Ma, L.; Ehrlich, S. N.; Zheng, W.; Epps, T. H., III; Korley, L. T. J.; Vlachos, D. G. Size and Structure Effects of Carbon-Supported Ruthenium Nanoparticles on Waste Polypropylene Hydrogenolysis Activity, Selectivity, and Product Microstructure. *ACS Catal.* **2024**, *14* (5), 3228−3240.
(50) Nakaji, Y.; Tamura, M.; Miyaoka, S.; Kumagai, S.; Tanji, M.; Nakagawa, Y.; Yoshioka, T.; Tomishige, K. Low-Temperature Catalytic Upgrading of Waste Polyolefinic Plastics into Liquid Fuels and Waxes. *Appl. Catal., B* **2021**, *285*, No. 119805.
(51) Ji, H.; Wang, X.; Wei, X.; Peng, Y.; Zhang, S.; Song, S.; Zhang, H. Boosting Polyethylene Hydrogenolysis Performance of Ru-CeO_2 Catalysts by Finely Regulating the Ru Sizes. *Small* **2023**, *19* (35), No. 2300903.
(52) Nakagawa, Y.; Oya, S.-i.; Kanno, D.; Nakaji, Y.; Tamura, M.; Tomishige, K. Regioselectivity and Reaction Mechanism of Ru-Catalyzed Hydrogenolysis of Squalane and Model Alkanes. *ChemSusChem* **2017**, *10* (1), 189−198.
(53) Hibbitts, D. D.; Flaherty, D. W.; Iglesia, E. Role of Branching on the Rate and Mechanism of C−C Cleavage in Alkanes on Metal Surfaces. *ACS Catal.* **2016**, *6* (1), 469−482.
(54) Wang, C.; Xie, T.; Kots, P. A.; Vance, B. C.; Yu, K.; Kumar, P.; Fu, J.; Liu, S.; Tsilomelekis, G.; Stach, E. A.; et al. Polyethylene Hydrogenolysis at Mild Conditions over Ruthenium on Tungstated Zirconia. *JACS Au* **2021**, *1* (9), 1422.
(55) Wang, C.; Yu, K.; Sheludko, B.; Xie, T.; Kots, P. A.; Vance, B. C.; Kumar, P.; Stach, E. A.; Zheng, W.; Vlachos, D. G. A General Strategy and a Consolidated Mechanism for Low-Methane Hydrogenolysis of Polyethylene over Ruthenium. *Appl. Catal., B* **2022**, *319*, No. 121899.
(56) Kots, P. A.; Liu, S.; Vance, B. C.; Wang, C.; Sheehan, J. D.; Vlachos, D. G. Polypropylene Plastic Waste Conversion to Lubricants over Ru/TiO_2 Catalysts. *ACS Catal.* **2021**, *11*, 8104−8115.
(57) Kots, P. A.; Xie, T.; Vance, B. C.; Quinn, C. M.; de Mello, M. D.; Boscoboinik, J. A.; Wang, C.; Kumar, P.; Stach, E. A.; Marinkovic, N. S.; et al. Electronic Modulation of Metal-Support Interactions Improves Polypropylene Hydrogenolysis over Ruthenium Catalysts. *Nat. Commun.* **2022**, *13* (1), 5186.
(58) Jaydev, S. D.; Martín, A. J.; Pérez-Ramírez, J. Direct Conversion of Polypropylene into Liquid Hydrocarbons on Carbon-Supported Platinum Catalysts. *ChemSusChem* **2021**, *14* (23), 5179−5185.

https://doi.org/10.1021/jacsau.4c00289
JACS Au 2024, 4, 2081−2098

(59) Kang, Q.; Chu, M.; Xu, P.; Wang, X.; Wang, S.; Cao, M.; Ivasenko, O.; Sham, T.-K.; Zhang, Q.; Sun, Q.; et al. Entropy Confinement Promotes Hydrogenolysis Activity for Polyethylene Upcycling. *Angew. Chem., Int. Ed.* **2023**, *62* (47), No. e202313174.
(60) Chu, M.; Wang, X.; Wang, X.; Lou, X.; Zhang, C.; Cao, M.; Wang, L.; Li, Y.; Liu, S.; Sham, T.-K.; et al. Site-Selective Polyolefin Hydrogenolysis on Atomic Ru for Methanation Suppression and Liquid Fuel Production. *Research* **2023**, *6*, No. 0032.
(61) Peczak, I. L.; Kennedy, R. M.; Hackler, R. A.; Wang, R.; Shin, Y.; Delferro, M.; Poeppelmeier, K. R. Scalable Synthesis of $Pt/SrTiO_3$ Hydrogenolysis Catalysts in Pursuit of Manufacturing-Relevant Waste Plastic Solutions. *ACS Appl. Mater. Interfaces* **2021**, *13* (49), 58691−58700.
(62) McCullough, K. E.; Peczak, I. L.; Kennedy, R. M.; Wang, Y.-Y.; Lin, J.; Wu, X.; Paterson, A. L.; Perras, F. A.; Hall, J.; Kropf, A. J.; et al. Synthesis of Platinum Nanoparticles on Strontium Titanate Nanocuboids via Surface Organometallic Grafting for the Catalytic Hydrogenolysis of Plastic Waste. *J. Mater. Chem. A* **2023**, *11* (3), 1216−1231.
(63) Quignard, F.; Le'cuyer, C.; Choplin, A. s.; Olivier, D. l.; Basset, J.-M. Surface Organometallic Chemistry of Zirconium: Application to the Stoichiometric Activation of the C−H Bonds of Alkanes and to the Low-Temperature Catalytic Hydrogenolysis of Alkanes. *J. Mol. Catal.* **1992**, *74* (1), 353−363.
(64) Dufaud, V.; Basset, J. M. Catalytic hydrogenolysis at low temperature and pressure of polyethylene and polypropylene to diesels or lower alkanes by a zirconium hydride supported on silica-alumina: A step toward polyolefin degradation by the microscopic reverse of Ziegler-Natta polymerization. *Angew. Chem. -Int. Ed.* **1998**, *37* (6), 806−810.
(65) Norsic, S.; Larabi, C.; Delgado, M.; Garron, A.; de Mallmann, A.; Santini, C.; Szeto, K. C.; Basset, J.-M.; Taoufik, M. Low Temperature Hydrogenolysis of Waxes to Diesel Range Gasoline and Light Alkanes: Comparison of Catalytic Properties of Group 4, 5 and 6 Metal Hydrides Supported on Silica−Alumina. *Catal. Sci. Technol.* **2012**, *2* (1), 215−219.
(66) Chen, S.; Tennakoon, A.; You, K.-E.; Paterson, A. L.; Yappert, R.; Alayoglu, S.; Fang, L.; Wu, X.; Zhao, T. Y.; Lapak, M. P.; et al. Ultrasmall Amorphous Zirconia Nanoparticles Catalyse Polyolefin Hydrogenolysis. *Nat. Catal.* **2023**, *6* (2), 161−173.
(67) Chauhan, M.; Antil, N.; Rana, B.; Akhtar, N.; Thadhani, C.; Begum, W.; Manna, K. Isoreticular Metal−Organic Frameworks Confined Mononuclear Ru-Hydrides Enable Highly Efficient Shape-Selective Hydrogenolysis of Polyolefins. *JACS Au* **2023**, *3* (12), 3473−3484.
(68) Tang, X.; Yu, A.; Yang, Q.; Yuan, H.; Wang, Z.; Xie, J.; Zhou, L.; Guo, Y.; Ma, D.; Dai, S. Significance of Epitaxial Growth of PtO_2 on Rutile TiO_2 for Pt/TiO_2 Catalysts. *J. Am. Chem. Soc.* **2024**, *146* (6), 3764−3772.

https://doi.org/10.1021/jacsau.4c00289
JACS Au 2024, 4, 2081−2098